

Filling an empty lattice by local injection of quantum particles

Akash Trivedi,^{1,2,*} Sparsh Gupta,^{2,†} Bijay Kumar Agarwalla^{Ⓜ,1,‡} Abhishek Dhar,^{2,§}
Manas Kulkarni,^{2,¶} Anupam Kundu,^{2,**} and Sanjib Sabhapandit^{Ⓜ,3,††}

¹*Department of Physics, Indian Institute of Science Education and Research Pune,*

Dr. Homi Bhabha Road, Ward No. 8, NCL Colony, Pashan, Pune, Maharashtra 411008, India

²*International Centre for Theoretical Sciences, Tata Institute of Fundamental Research, Bangalore 560089, India*

³*Raman Research Institute, Bangalore 560080, India*



(Received 18 October 2022; accepted 6 October 2023; published 2 November 2023)

We study the quantum dynamics of filling an empty lattice of size L by connecting it locally with an equilibrium thermal bath that injects noninteracting bosons or fermions. We adopt four different approaches, namely, (i) direct exact numerics, (ii) Redfield equation, (iii) Lindblad equation, and (iv) quantum Langevin equation, which are unique in their ways for solving the time dynamics and the steady state. In this simple setup we investigate open quantum dynamics and subsequent approach to thermalization. The quantities of interest that we consider are the spatial density profile and the total number of bosons and fermions in the lattice. The spatial spread is ballistic in nature and the local occupation eventually settles down owing to equilibration. The ballistic spread of local density admits a universal scaling form. We show that this universality is only seen when the condition of detailed balance is satisfied by the baths. The difference between bosons and fermions shows up in the early time growth rate and the saturation values of the profile. The techniques developed here are applicable to systems in arbitrary dimensions and for arbitrary geometries.

DOI: [10.1103/PhysRevA.108.052204](https://doi.org/10.1103/PhysRevA.108.052204)

I. INTRODUCTION

Understanding quantum dynamics and subsequent thermalization of a system in the presence of a bath is an interesting question in open quantum systems both from a fundamental and an applied perspective [1–6]. In this regard, a plethora of studies have emerged in successfully addressing some of the pressing issues [7,8]. A good starting point for such an investigation is to understand the quantum dynamics and subsequent equilibration that an empty lattice would undergo when attached to a reservoir. An intricate interplay between Hermitian, non-Hermitian dynamics (arising due to finite system-reservoir coupling), and quantum statistics can lead to highly nontrivial dynamics and steady state.

In this direction, there have been several works on the quantum dynamics of open systems. A specific class of such investigations includes studies of systems attached to localized sources or sink. In particular, Refs. [9–17] focused on understanding the dynamics of various classes of quantum systems subject to localized losses. Another complementary set of works studied localized injection in initially empty lattices [18–21]. Given the complexity of such setups, one is often compelled to resort to approximations such as weak

system-reservoir coupling and separation of timescales between system and reservoir dynamics. Albeit quite successful [18,19], these approximations might miss certain key aspects of quantum dynamics and thermalization. For example, a non-monotonic behavior of out-of-equilibrium transport properties when one tunes the system-reservoir coupling from weak to strong may be missed in traditional perturbative approaches. Furthermore, the assumption of well-separated reservoir and system timescales can become invalid for a wide class of baths with spectral functions of nonanalytical type [22]. Therefore, it is crucial to employ exact approaches to investigate such setups.

In this work, we consider a one-dimensional empty lattice (system) of size L coupled to a boson and fermion reservoir at a particular site. Some natural questions that come to mind are as follows: How many particles are there in the lattice at a particular time? What is the space resolved density profile at any given time snapshot? How does the density profile spread with time? In our work, we study quantum dynamics of (i) the local density profile on the lattice $n_i(t)$ and (ii) the total number of bosons and fermions on the lattice $N(t) = \sum_{i=1}^L n_i(t)$, and their subsequent thermalization (or lack thereof) properties. A schematic of our setup is given in Fig. 1. We employ four methods which are unique in their own ways and offer complementary benefits: (i) direct exact numerics for correlation matrix, (ii) Redfield equation (perturbative and Markovian), (iii) local Lindblad equation (perturbative, Markovian, and weak intersite hopping), and (iv) exact quantum Langevin equation. The summary of our work is as follows:

(1) The initial growth for the total occupation $N(t)$ for bosons and fermions is linear in time and it subsequently saturates (for a finite lattice size) to a constant value in an

*akash.trivedi@students.iiserpune.ac.in

†sparsh.gupta@icts.res.in

‡bijay@iiserpune.ac.in

§abhishek.dhar@icts.res.in

¶manas.kulkarni@icts.res.in

**anupam.kundu@icts.res.in

††sanjib@rri.res.in

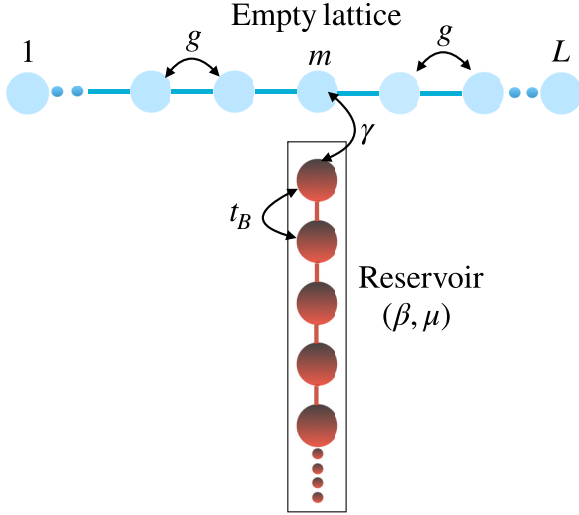


FIG. 1. Schematic of our setup: an empty (blue) one-dimensional lattice of size L is connected to a reservoir (red) at a particular site. The reservoir is coupled to the lattice at a particular site, represented by m . The intersite hopping parameter within the lattice (within the reservoir) is g (t_B). The coupling between the lattice and the reservoir is denoted by γ . The reservoir is maintained in equilibrium at an inverse temperature β and chemical potential μ .

exponential fashion (Fig. 2). For infinite lattice there is no saturation and $N(t) \propto t \forall t$ (Fig. 3).

(2) The local spatial density profile $n_i(t)$ exhibits a ballistic spread for both bosons (Figs. 5 and 6) and fermions (Figs. 19 and 20). For finite lattice, at a given site, $n_i(t)$ initially grows in time and eventually saturates owing to equilibration with the bath for bosons (Fig. 4) and fermions (Fig. 18).

(3) We observe a much slower accumulation of fermions in comparison to bosons (Fig. 17) which is rooted in quantum statistics (Pauli exclusion principle). Albeit there is an analogy between fermions and classical exclusion processes, there are interesting differences [23,24] for the case of fermions which are intrinsically quantum in nature. For example, the spread of the density profile in the classical exclusion case is diffusive in contrast to the ballistic spread for the quantum case.

(4) Our microscopic starting point is drastically different from the phenomenological approaches such as unidirectional filling [18,19] and therefore lacking the detailed balance condition. In our work, we argue that this detailed balance condition plays a paramount role in deciding the fate of the dynamics. Nonetheless, the techniques developed in Refs. [18,19] can be adapted to obtain analytical forms for spatial density profile (Figs. 15 and 16).

(5) In a suitable parameter regime, we find that the spatial density profile in the ballistic regime possesses a universal scaling form [Eqs. (60) and (61)], valid for both bosons and fermions.

The plan of the paper is as follows: In Sec. II, we first introduce the setup and discuss the four methods. In Sec. III, we present our findings for bosons using all four methods. In Sec. IV, we briefly discuss our findings for fermions obtained from exact numerics. In Sec. V, we place our work in the context of recent works and provide a detailed comparison.

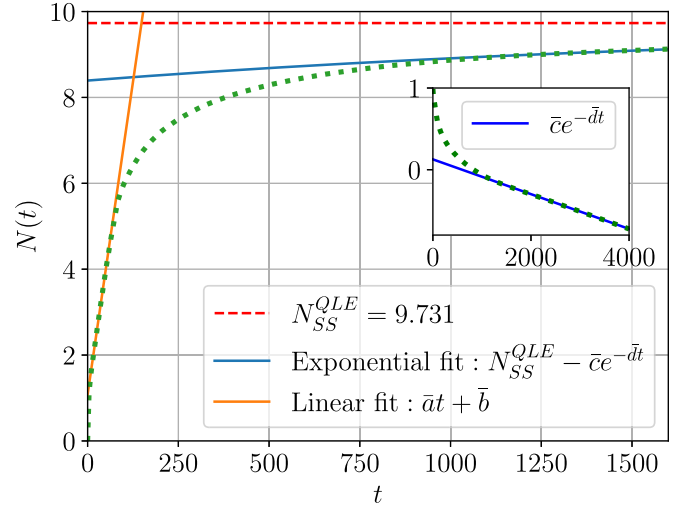


FIG. 2. Behavior of total occupation $N(t)$ [Eq. (7)] versus t for system size $L = 40$ for the bosonic case, using direct exact numerics as described in Sec. II A. The bath is connected at site number $m = 21$. The linear early-time growth and exponential late-time saturation can be clearly seen. Red dashed line shows the steady-state value N_{SS}^{QLE} obtained from exact quantum Langevin equation approach, described in Sec. II D. The parameters are $g = 0.5$, $\gamma = 1$, $t_B = 1$, $\beta = 1$, and $\mu = -2.01$. Note that the fitting parameters for the early-time linear growth $\bar{a}t + \bar{b}$ are $\bar{a} = 0.058$, $\bar{b} = 1.082$. For the late-time behavior, the fitting parameters for the exponential relaxation $N_{SS}^{QLE} - \bar{c}e^{-\bar{d}t}$ are $\bar{c} = 1.359$, $\bar{d} = 4.95 \times 10^{-4}$ with N_{SS}^{QLE} chosen to be same as the steady-state value obtained from QLE ($N_{SS}^{QLE} = 9.731$). This implies that for $L = 40$, the timescale to reach steady state is $t_{SS} = 1/\bar{d} \sim 2000$. The inset shows the plot for $[\ln(N_{SS}^{QLE} - N(t))]$ vs t (green dots) and it clearly demonstrates the long-time exponential relaxation in time towards the steady state. We choose $\gamma = 1$ (nonperturbative regime in system-bath coupling) to ensure that the system relaxes towards steady state relatively fast. For this figure, the system size $L = 40$ is chosen such that both the early-time linear behavior and long-time exponential behavior are clearly visible.

Finally, we summarize our results along with an outlook in Sec. VI. We delegate some details to the Appendix.

II. SETUP AND METHODOLOGY

In this section, we discuss our microscopic model for the injection of identical bosons and fermions in a one-dimensional lattice. The lattice initially is an empty tight-binding chain of L sites. The Hamiltonian of the lattice is given by (setting $\hbar = 1$ throughout the paper),

$$H_S = g \sum_{i=1}^{L-1} (a_i^\dagger a_{i+1} + a_{i+1}^\dagger a_i), \quad (1)$$

where a_i (a_i^\dagger) is the annihilation (creation) operator of the i th site of the lattice. The hopping parameter is denoted by g . We inject the particles at a particular site (for example, near the middle) of the lattice by putting it in contact with a reservoir which is represented by a semi-infinite tight-binding chain

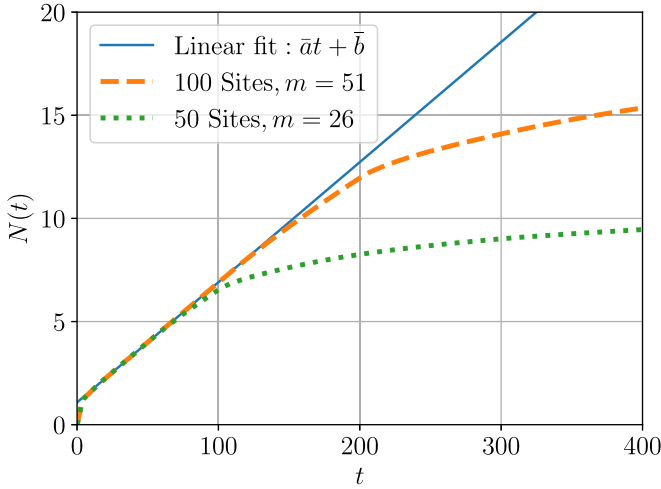


FIG. 3. Total occupation $N(t)$ [Eq. (7)] versus t for different system sizes using direct numerics as described in Sec. II A. The parameters used are $g = 0.5$, $t_B = 1$, $\beta = 1$, $\mu = -2.01$, and $\gamma = 1$ are exactly the same as in Fig. 2 except the system size. It can be seen that the deviation from the linear growth starts at a timescale that scales with the system size L . The fitting parameters are $\bar{a} = 0.058$, $\bar{b} = 1.082$.

whose Hamiltonian is given by

$$H_B = t_B \sum_{i=1}^{\infty} (b_i^\dagger b_{i+1} + b_{i+1}^\dagger b_i). \quad (2)$$

Here b_i (b_i^\dagger) is the annihilation (creation) operator of the i th site of the bath and t_B is the nearest-neighbor hopping

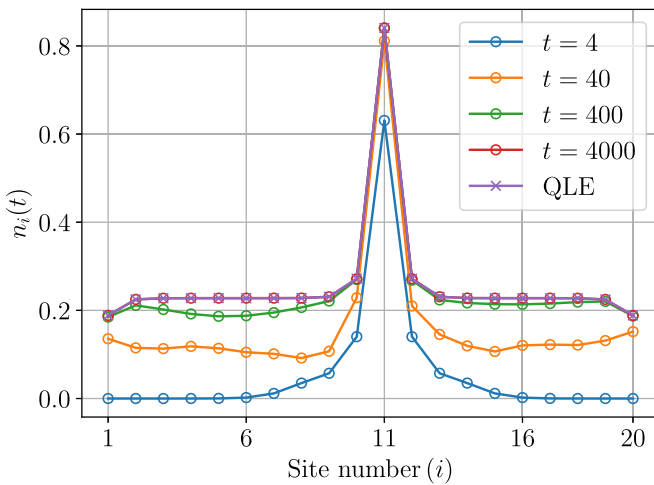


FIG. 4. Local density profile $n_i(t)$ [Eq. (6)] for bosons with $L = 20$ lattice sites with bath attached at a particular site ($m = 11$) for various time snapshots, using direct numerics (empty circles), as discussed in Sec. II A. The long-time limit of this density profile agrees perfectly with that obtained from QLE (cross), as discussed in Sec. II D. The parameters are $t_B = 1$, $g = 0.5$, $\beta = 1$, $\mu = -2.01$, and $\gamma = 1$. Note that apart from the system size the parameters chosen here are exactly the same as in Figs. 2 and 3. The system size $L = 20$ is chosen keeping in mind computational feasibility and to ensure a relatively quick approach to steady state.

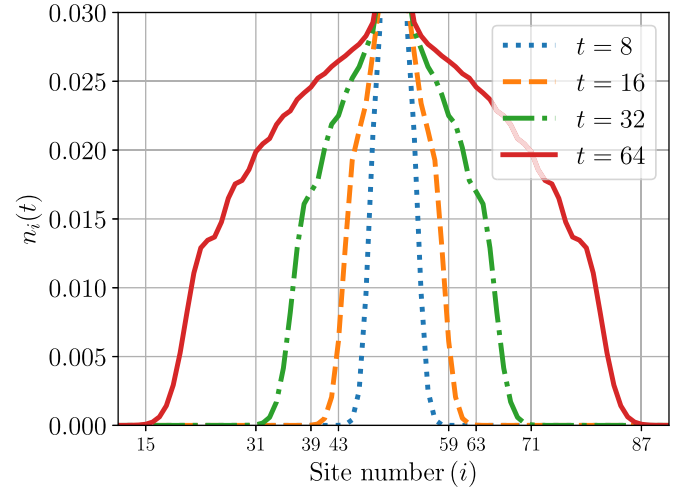


FIG. 5. Local density profile $n_i(t)$ [Eq. (6)] for bosons with $L = 100$ sites with bath attached at $m = 51$ from direct exact numerics, described in Sec. II A. We choose relatively short times to clearly demonstrate the ballistic growth of the density profile. Note that this front of the density profiles spreads with velocity $c = 2g$, where g is the intersite hopping within the lattice. This figure clearly indicates the presence of scaling which is demonstrated in Fig. 6. The parameters are $t_B = 1$, $g = 0.25$, $\beta = 1$, $\mu = -2.01$, and $\gamma = 1$. Note that the parameters chosen here are exactly the same as in Figs. 2–4 except the value of g . $g = 0.25$ is chosen here in order to illustrate ballistic spreading over a computationally feasible system size L .

between the bath sites. Note that a_i and b_i operators satisfy either commutation or anticommutation algebra for bosons or fermions, respectively. At $t = 0$, we switch on the coupling between the lattice and the bath which can be described by the following Hamiltonian:

$$H_{SB} = \gamma (a_m^\dagger b_1 + b_1^\dagger a_m), \quad (3)$$

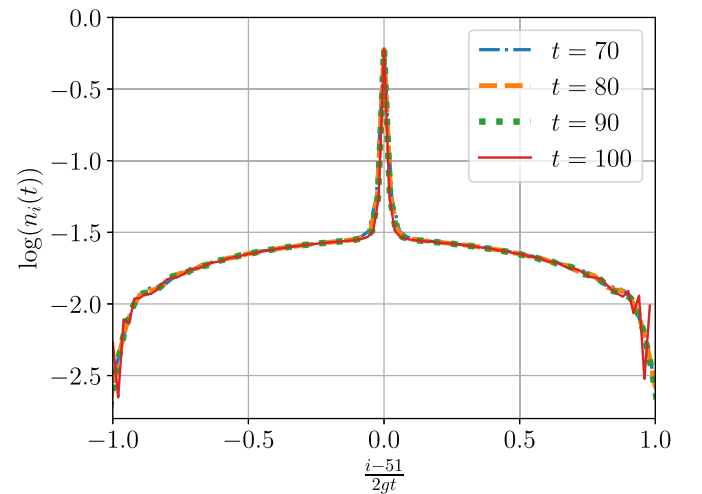


FIG. 6. A scaled plot of $\ln(n_i(t))$ [Eq. (6)] for $L = 100$ bosonic sites with bath attached at $m = 51$ from direct exact numerics to demonstrate the ballistic spread of spatial density profile $n_i(t)$ [Eq. (6)]. The parameters are $t_B = 1$, $g = 0.25$, $\beta = 1$, $\mu = -2.01$, and $\gamma = 1$. The logarithm mentioned in this plot is with base 10.

where γ is the coupling strength and the m th site of the lattice is coupled to the first site of the bath. In this work we choose $m = (N + 1)/2$ for odd N and $m = N/2 + 1$ for even N . The initial density operator $\rho(t = 0)$ for the setup is taken as a product state

$$\rho(0) = \rho_S(0) \otimes \rho_B^{\text{th}}(0) \quad (4)$$

with the lattice initially being empty, i.e., $\rho_S(t = 0) = |\mathbf{0}\rangle\langle\mathbf{0}|$ where $|\mathbf{0}\rangle$ denotes a state with all sites empty. In other words, the lattice is in vacuum. The bath density operator is in equilibrium at temperature $T = (k_B\beta)^{-1}$ where k_B is the Boltzmann constant henceforth set to 1 and chemical potential μ ,

$$\rho_B^{\text{th}} = \frac{e^{-\beta(H_B - \mu N_B)}}{Z}, \quad (5)$$

where N_B is the number operator for the bath and Z is the grand partition function for the bath. The superscript ‘‘th’’ in Eqs. (4) and (5) stands for thermal equilibrium.

With this generic setup in hand, our interest here is to study the quantum dynamics of the spatial density profile of bosons and fermions

$$n_i(t) = \langle a_i^\dagger(t) a_i(t) \rangle, \quad (6)$$

where we use the Heisenberg representation for the operators and $\langle \dots \rangle$ denotes an average over the initial density matrix $\rho(0)$. We also look at the total number of particles in the lattice

$$N(t) = \sum_{i=1}^L n_i(t). \quad (7)$$

In order to have a detailed understanding of the quantities given in Eqs. (6) and (7), we use four different approaches which we elaborate below.

A. Method 1: Exact quantum dynamics for correlation matrix

In this subsection, we discuss direct exact numerical calculations for computing the observables of interest. As the entire setup here is quadratic, the equations of motion for the two-point correlation functions involving both the system and bath degrees of freedom closes. Thus, the central idea here is to numerically evolve the two-point correlation function consisting of all the degrees of freedom via the single-particle Hamiltonian of the setup. Once this unitary propagation is performed, the quantities mentioned in Eqs. (6) and (7) can be suitably extracted. This procedure, of course, involves one to consider a large but finite bath.

Let L_B be the number of bath sites such that $L_B \gg L$. We write the full Hamiltonian for the setup as

$$H = H_S + H_B + H_{SB} = \sum_{i,j=1}^{L+L_B} h_{ij} d_i^\dagger d_j \equiv D^\dagger h D. \quad (8)$$

Here, $D = \{d_i\}$ is a column vector containing all the annihilation operators of the system and the bath. Specifically, $D \equiv \{a_1, a_2, \dots, a_L, b_1, b_2, \dots, b_{L_B}\}$. Naturally, $D^\dagger = \{d_i^\dagger\}$ is the row vector consisting of all the creation operators of the system and the bath. h is the single-particle Hamiltonian of the full setup and has dimension $(L + L_B) \times (L + L_B)$. Since our central focus here is to study the filling of lattice system,

we will not require the information of the full density matrix. Instead, we will just need to focus on the correlation matrix

$$S(t) = \langle [D^\dagger(t)]^T [D^T(t)] \rangle, \quad (9)$$

where the superscript T stands for the transpose of a matrix. The matrix element of S is given as

$$S_{ij}(t) = \langle d_i^\dagger(t) d_j(t) \rangle. \quad (10)$$

Following the Heisenberg equation of motion $i \frac{d}{dt} O = [O, H]$, for any operator $O(t)$, one can write

$$\frac{d}{dt} (d_i^\dagger d_j) = i[H, d_i^\dagger d_j] = i \sum_{r,s=1}^{L+L_B} h_{rs} [d_r^\dagger d_s, d_i^\dagger d_j]. \quad (11)$$

Using the commutation and anticommutation relations for bosons and fermions, respectively, Eq. (11) can be simplified to

$$\frac{d}{dt} (d_i^\dagger d_j) = i \sum_{r=1}^{L+L_B} (h_{ri} d_r^\dagger d_j - h_{jr} d_i^\dagger d_r). \quad (12)$$

Equation (12) holds for both bosons and fermions. Using Eq. (12), and the fact that the single-particle Hamiltonian h is symmetric, we can obtain the evolution for the correlation matrix element of $S(t)$, which is given by [25–27]

$$\dot{S}_{ij}(t) = i \sum_{r=1}^{L+L_B} (h_{ir} S_{rj}(t) - S_{ir}(t) h_{rj}) = i[h, S(t)]_{ij}, \quad (13)$$

the solution of which is given by

$$S(t) = e^{iht} S(0) e^{-iht}, \quad (14)$$

where we recall that h is the single-particle Hamiltonian for the full setup. Equation (14) holds for both bosons and fermions. We can easily construct the initial correlation matrix $S(0)$ from the initial density operator $\rho(0)$. Since the lattice chain is initially in vacuum and is decoupled from the bath, all the two-point correlations of the form $\langle a_i^\dagger(0) a_j(0) \rangle$, $\langle a_i^\dagger(0) b_j(0) \rangle$, and $\langle b_i^\dagger(0) a_j(0) \rangle$ will be zero. The nonzero entries in $S(0)$ are the two-point correlations of the bath degrees of freedom and of the form $\langle b_i^\dagger(0) b_j(0) \rangle$. These entries can be obtained as follows. We recall that the bath Hamiltonian given in Eq. (2) can be expressed as

$$H_B = \sum_{i,j=1}^{L_B} h_{ij}^B b_i^\dagger b_j, \quad (15)$$

where h^B is the single-particle Hamiltonian of the bath. This Hamiltonian can be easily diagonalized by a unitary transformation U , i.e., $h^B = U \Lambda_B U^\dagger$ with Λ_B being a diagonal matrix with single-particle eigenvalues as its entries. The Hamiltonian in the diagonal form can be written as

$$H_B = \sum_{q=1}^{L_B} \lambda_q^B b_q^\dagger b_q, \quad (16)$$

where

$$b_i = \sum_{q=1}^{L_B} U_{iq} b_q \quad (17)$$

with b_q being the annihilation operator of q th normal mode of the bath with eigenvalues λ_q^B . One can then easily find that

$$\langle b_i^\dagger(0)b_j(0) \rangle^{\text{th}} = \sum_{q=1}^{L_B} U_{iq}^* U_{jq} \bar{n}(\lambda_q^B), \quad (18)$$

where we have used the fact that $\langle b_q^\dagger b_{q'} \rangle = \bar{n}(\lambda_q^B) \delta_{qq'}$. Here $\bar{n}(\omega)$ can either be Bose or Fermi function and is given by

$$\bar{n}(\omega) = \frac{1}{e^{\beta(\omega-\mu)} \pm 1}, \quad (19)$$

where $-$ and $+$ stand for bosons and fermions, respectively. With $S(t=0)$ constructed from all these initial correlations, we can now propagate the correlation matrix following Eq. (14) and suitably extract the required entries from $S(t)$ to compute $n_i(t)$ and thereby $N(t)$, as defined in Eqs. (6) and (7), respectively. It should be noted that if $L_B \gg L$, then the system dynamics is almost equivalent to that when subjected to a true bath with infinite degrees of freedom.

Since this exact numerical recipe involves unitary evolution with respect to the Hamiltonian of the entire setup [see Eq. (8)], it can become computationally difficult if the total size $L + L_B$ is large. Therefore, it is useful to study time dynamics for this setup following complementary approaches, namely, the Redfield and Lindblad master equations which are perturbative and Markovian in nature. This procedure involves integrating out infinite degrees of freedom of the bath and thereby providing an effective dynamical description for the reduced density matrix of the lattice system which can then be used to study lattices with a large number of sites.

B. Method 2: Redfield quantum master-equation approach

In this subsection, we discuss the Redfield equation and provide the key steps that are involved to obtain the spatial

density profile and total number of particles. We start by writing the system-bath interaction Hamiltonian, given in Eq. (3), in the interaction picture as

$$H_{\text{SB}}^I(t) = e^{iH_0 t} H_{\text{SB}} e^{-iH_0 t} = \gamma (a_m^\dagger(t) b_1(t) + b_1^\dagger(t) a_m(t)), \quad (20)$$

where $H_0 = H_S + H_B$ and

$$a_m(t) = e^{iH_S t} a_m e^{-iH_S t}; \quad b_1(t) = e^{iH_B t} b_1 e^{-iH_B t}. \quad (21)$$

Starting from the exact von Neumann equation, one can write an exact equation governing the dynamics of the reduced density matrix for the system in the interaction picture as

$$\frac{d}{dt} \rho_{\text{SI}}(t) = - \int_0^t d\tau \text{Tr}_B [H_{\text{SB}}^I(t), [H_{\text{SB}}^I(\tau), \rho_I(\tau)]], \quad (22)$$

where $\rho_I(\tau)$ is the full density operator in the interaction picture. The subscript ‘‘SI’’ in Eq. (22) stands for system and interaction picture, respectively. Now to arrive at the Redfield equation, one assumes (i) weak system-bath coupling limit (Born approximation) and (ii) Markovian limit [1,2,28]. The Born approximation implies writing $\rho_I(\tau)$ in Eq. (22) as a direct product state of the system and the bath density matrix, i.e., $\rho_I(\tau) = \rho_{\text{SI}}(\tau) \otimes \rho_B^{\text{th}}$ where ρ_B^{th} is defined in Eq. (5). The Markov approximation involves changing $\rho_{\text{SI}}(\tau)$ to $\rho_{\text{SI}}(t)$ and further extending the upper limit of the integral t to ∞ , in Eq. (22). The Markovian approximation used here can be justified under a separation of bath and system timescales. In particular, the Markovian approximation is valid for system timescales much larger than the decay timescale of the bath. After some algebraic manipulations, we obtain the Redfield equation as [27]

$$\frac{d}{dt} \rho_{\text{SI}}(t) = -\gamma^2 \int_0^\infty d\tau [\langle b_1(t) b_1^\dagger(\tau) \rangle [a_m^\dagger(t), a_m(\tau) \rho_{\text{SI}}(t)] + \langle b_1^\dagger(\tau) b_1(t) \rangle [\rho_{\text{SI}}(t) a_m(\tau), a_m^\dagger(t)] + \text{H.c.}]. \quad (23)$$

In the Schrödinger picture, we receive

$$\frac{d}{dt} \rho_{\text{SS}}(t) = i[\rho_{\text{SS}}(t), H_S] - \gamma^2 \int_0^\infty d\tau [\langle b_1(t) b_1^\dagger(\tau) \rangle [a_m^\dagger, a_m(\tau - t) \rho_{\text{SS}}(t)] + \langle b_1^\dagger(\tau) b_1(t) \rangle [\rho_{\text{SS}}(t) a_m(\tau - t), a_m^\dagger] + \text{H.c.}], \quad (24)$$

where the subscript ‘‘SS’’ in Eq. (24) stands for system and Schrödinger picture, respectively. Since the bath operators are defined in the interaction picture, the corresponding two-point correlation functions are known exactly and as before [see Eq. (18)] can be written in terms of the normal modes of the bath as

$$\begin{aligned} \langle b_1^\dagger(\tau) b_1(t) \rangle &= \sum_q |U_{1q}|^2 e^{-i\lambda_q^B(t-\tau)} \bar{n}(\lambda_q^B), \\ \langle b_1(t) b_1^\dagger(\tau) \rangle &= \sum_q |U_{1q}|^2 e^{-i\lambda_q^B(t-\tau)} [1 \pm \bar{n}(\lambda_q^B)], \end{aligned} \quad (25)$$

where recall that λ_q^B is the eigenvalue of the q th mode of the bath and $\bar{n}(\omega)$ is defined in Eq. (19). In Eq. (25), the \pm stands for bosons and fermions, respectively. We now express the

above Redfield equation in Eq. (24) in terms of the eigenoperators of the system Hamiltonian. In other words, we first diagonalize the lattice Hamiltonian H_S and write

$$H_S = \sum_{i,j=1}^L h_{ij}^S a_i^\dagger a_j = \sum_{k=1}^L \lambda_k^S a_k^\dagger a_k, \quad (26)$$

where

$$h^S = W \Lambda_S W^\dagger \quad (27)$$

and therefore the matrix W is responsible for diagonalizing the single-particle system Hamiltonian H_S and Λ_S is the diagonal matrix containing the single-particle eigenvalues of the

system. Here

$$a_i = \sum_{k=1}^L W_{ik} a_k. \quad (28)$$

Following this diagonalization procedure and using Eqs. (24) and (25), we can rewrite the Redfield equation as [27]

$$\dot{\rho}_{SS}(t) = i[\rho_{SS}(t), H_S] - \sum_{k,k'=1}^L \int_{-\infty}^{\infty} \frac{d\omega}{2\pi} [I(\omega) \mathcal{L}(\rho_{SS}) + \text{H.c.}], \quad (29)$$

where

$$I(\omega) = \int_0^{\infty} d\tau e^{-i(\omega - \lambda_k^S)\tau} \quad (30)$$

and

$$\begin{aligned} \mathcal{L}(\rho_{SS}) = & [f_{kk'}(\omega) \pm F_{kk'}(\omega)][a_k^\dagger, a_{k'} \rho_{SS}(t)] \\ & + F_{kk'}(\omega)[\rho_{SS}(t) a_{k'}^\dagger, a_k^\dagger]. \end{aligned} \quad (31)$$

The functions $f_{kk'}(\omega)$ and $F_{kk'}(\omega)$ in Eq. (31) are defined as

$$\begin{aligned} f_{kk'}(\omega) &= W_{mk}^* W_{mk'} J(\omega), \\ F_{kk'}(\omega) &= W_{mk}^* W_{mk'} J(\omega) \bar{n}(\omega), \end{aligned} \quad (32)$$

where recall that the index m in W_{mk} refers to the m th site of the lattice system that is connected with the bath [see Eq. (3)]. Note that the \pm sign in Eq. (31) again refers to the boson and fermion cases. Here, $J(\omega)$ is the spectral density of the bath, defined as

$$J(\omega) \equiv 2\pi \gamma^2 \sum_q |U_{1q}|^2 \delta(\omega - \lambda_q^B). \quad (33)$$

Note that the two-point correlation functions of the system are given as

$$C_{k,k'}(t) = \langle a_k^\dagger(t) a_{k'}(t) \rangle = \text{Tr}[a_k^\dagger(0) a_{k'}(0) \rho_{SS}(t)]. \quad (34)$$

From the Redfield equation [Eq. (29)], one can write a differential equation for the two-point correlation function defined in Eq. (34) as [29–31]

$$\begin{aligned} \frac{dC_{k,k'}(t)}{dt} = & i\lambda_k^S C_{k,k'}(t) + \frac{1}{2} \left[\tilde{F}_{k'k} - \sum_{\bar{k}=1}^L \tilde{f}_{k'\bar{k}} C_{k,\bar{k}}(t) \right] \\ & + (k \iff k')^\dagger, \end{aligned} \quad (35)$$

where $(k \iff k')^\dagger$ is a short form for the right-hand side of Eq. (35) when k and k' are interchanged and the terms are subjected to complex conjugation. The new functions (denoted by the symbol tilde) in Eq. (35) are defined as

$$\tilde{f}_{k'\bar{k}} = f_{k'\bar{k}}(\lambda_{\bar{k}}^S) - iP \int_{-\infty}^{\infty} \frac{d\omega}{\pi} \frac{f_{k'\bar{k}}(\omega)}{\omega - \lambda_{\bar{k}}^S}, \quad (36)$$

$$\tilde{F}_{k'k} = F_{k'k}(\lambda_k^S) - iP \int_{-\infty}^{\infty} \frac{d\omega}{\pi} \frac{F_{k'k}(\omega)}{\omega - \lambda_k^S}. \quad (37)$$

Here P refers to the Cauchy principal value. This particular form in Eqs. (36) and (37) is obtained by writing $I(\omega)$ in Eq. (30) using the Sokhotski-Plemelj theorem. Equation (35) forms a closed set of differential equations for the two-point correlation function which can be solved numerically

by grouping the equations in a matrix equation form. We therefore write the components of $C_{k,k'}(t)$ as a column vector with elements \mathbf{C}_r , $r = 1, 2, \dots, L^2$, and denote it by $\vec{\mathbf{C}}(t)$, and write Eq. (35) as

$$\frac{d\vec{\mathbf{C}}}{dt} = M\vec{\mathbf{C}} + \vec{\mathbf{Q}}, \quad (38)$$

where M is the homogeneous part and is a $L^2 \times L^2$ matrix and $\vec{\mathbf{Q}}$ is a $L^2 \times 1$ column vector. Note that the information about the quantum statistics is encoded only in the column vector $\vec{\mathbf{Q}}$ as a consequence of which the quantum dynamics of fermions and bosons differ. The formal solution to Eq. (38) with the initial condition $\vec{\mathbf{C}}(0) = 0$ (note that the lattice is initially empty) is given by

$$\vec{\mathbf{C}}(t) = \int_0^t d\tau e^{M(t-\tau)} \vec{\mathbf{Q}}. \quad (39)$$

We now write the solution in Eq. (39) more explicitly. To do so, we first diagonalize M as $M = V \Lambda_M V^{-1}$, and obtain

$$\begin{aligned} \mathbf{C}_r(t) &= \int_0^t d\tau \sum_{\alpha,s=1}^{L^2} V_{r\alpha} e^{\lambda_\alpha^M(t-\tau)} V_{\alpha s}^{-1} \mathbf{Q}_s \\ &= \sum_{\alpha,s=1}^{L^2} \left(\frac{e^{\lambda_\alpha^M t} - 1}{\lambda_\alpha^M} \right) V_{r\alpha} V_{\alpha s}^{-1} \mathbf{Q}_s. \end{aligned} \quad (40)$$

The real part of the eigenvalues $\{\lambda_\alpha^M\}$ of M matrix are in general expected to be all negative which would ensure a well-defined steady state in the long-time limit. When this gets violated, Redfield description is rendered unphysical and can happen for some set of parameters (e.g., large system-bath coupling). We now study the short- and long-time limits of $\mathbf{C}_r(t)$. Let us denote the eigenvalue with the largest magnitude as λ_L and the one with the smallest real part magnitude as λ_S . In the short-time limit ($t \ll 1/|\lambda_L|$), we can do a Taylor expansion and find that all two-point correlations grow linearly with time, thus,

$$\mathbf{C}_r(t \ll 1) = \chi_r t + O(t^2), \quad (41)$$

with a slope

$$\chi_r = \left(\sum_{\alpha,s=1}^{L^2} V_{r\alpha} V_{\alpha s}^{-1} \mathbf{Q}_s \right) = \mathbf{Q}_r. \quad (42)$$

We now discuss the long-time limit, i.e., $t \rightarrow \infty$. Note that Eq. (40) can be recasted as

$$\mathbf{C}_r = \mathbf{C}_r^{\text{SS}} + \sum_{\alpha,s=1}^{L^2} V_{r\alpha} V_{\alpha s}^{-1} \mathbf{Q}_s \frac{e^{\lambda_\alpha^M t}}{\lambda_\alpha^M}, \quad (43)$$

where the steady-state correlation elements ($t \rightarrow \infty$) are given by

$$\mathbf{C}_r^{\text{SS}} = - \sum_{\alpha,s=1}^{L^2} \frac{V_{r\alpha} V_{\alpha s}^{-1} \mathbf{Q}_s}{\lambda_\alpha^M} = -(M^{-1} \vec{\mathbf{Q}})_r, \quad (44)$$

and the second term in Eq. (43) indicates a long-time exponential approach to the steady state. The eigenvalue λ_S , with the smallest magnitude for the real part, will determine the

timescale $1/|\text{Re}[\lambda_S]|$, for convergence to the steady state. As the correlation functions are obtained in the diagonalized basis to determine the spatial density profile, the final step is to come back to the local site basis which gives

$$n_i(t) = \langle a_i^\dagger(t) a_i(t) \rangle = \sum_{k,k'=1}^L W_{ik'} W_{ik}^* C_{k,k'}(t), \quad (45)$$

where recall that $C_{k,k'}$ is defined in Eq. (34). The total particle number is given by summing over all lattice sites

$$N(t) = \sum_{k=1}^L C_{k,k}(t), \quad (46)$$

which at early times ($t \ll 1$) gives

$$N(t) \approx t \sum_{k=1}^L Q_{k,k} = t \sum_{k=1}^L \tilde{F}_{k,k} \quad (47)$$

$$= t \sum_{k=1}^L |W_{mk}|^2 J(\lambda_k^S) \bar{n}(\lambda_k^S). \quad (48)$$

Equation (47) clearly demonstrates an early-time linear growth with different slopes for fermions and bosons. In the limiting case with very small intersite hopping g , one can set $\lambda_k^S \approx 0$ (the eigenvalues of uncoupled lattice sites), as a result of which we get

$$N(t) \approx t J(0) \bar{n}(0). \quad (49)$$

We will later see that this is exactly what one receives from the local Lindblad equation. Note that in a suitable parameter regime, the Redfield approach can be simplified to a local Lindblad equation. As we will show in the next subsection (Sec. IIC), this allows for elegant analytical expressions for the local density $n_i(t)$ in Eq. (6) and the total occupation $N(t)$ in Eq. (7).

C. Method 3: Lindblad approach

In this subsection, we outline the Lindblad approach and present our results for local density $n_i(t)$ in Eq. (6) and total occupation $N(t)$ in Eq. (7). A common way to model open quantum systems that mimics incoherent processes is via the local Lindblad formalism [27,32–35] which is of the form

$$\dot{\rho}_{SS}(t) = i[\rho_{SS}, H_S] + \mathcal{D}[\rho_{SS}(t)], \quad (50)$$

where \mathcal{D} is the Lindbladian and is given by

$$\mathcal{D}[\rho_{SS}(t)] = 2 \mathcal{O} \rho_{SS} \mathcal{O}^\dagger - \{\mathcal{O}^\dagger \mathcal{O}, \rho_{SS}\}, \quad (51)$$

where we recall that $\rho_{SS}(t)$ is the reduced system density matrix in the Schrödinger picture and H_S is the system Hamiltonian, given in Eq. (1). Here \mathcal{O} represents different channels of openness of the lattice system. For our setup, if we derive a local Lindblad equation starting from the fully microscopic system-reservoir Hamiltonian [Eqs. (1)–(3)], both incoherent pump and loss terms naturally arise in the Lindbladian given in Eq. (50). More explicitly, the systematically derived local Lindblad equation [27,32–35] is given as

$$\begin{aligned} \dot{\rho}_{SS} = & i[\rho_{SS}, H_S] + \Gamma_G [2a_m^\dagger \rho_{SS} a_m - \{a_m a_m^\dagger, \rho_{SS}\}] \\ & + \Gamma_L [2a_m \rho_{SS} a_m^\dagger - \{a_m^\dagger a_m, \rho_{SS}\}], \end{aligned} \quad (52)$$

where the gain Γ_G and the loss Γ_L coefficients are given by

$$\Gamma_G = \frac{J(0)}{2} \bar{n}(0), \quad (53)$$

$$\Gamma_L = \frac{J(0)}{2} [1 \pm \bar{n}(0)]. \quad (54)$$

Recall that $J(\omega)$ is the spectral density of the bath, defined in Eq. (33). Note that the zeros in the argument of $J(0)$ and $\bar{n}(0)$ in Eqs. (53) and (54) are due to the fact that there is no onsite term in the system Hamiltonian given in Eq. (1). The \pm sign in Eq. (54) stands for bosons and fermions, respectively. It is important to highlight that the validity of the local Lindblad equation in Eq. (52) relies on weak system bath coupling γ as well as weak intersite hopping parameter g within the lattice system [27].

Following Eq. (52) one can write the equations of motion for the two-point correlation functions of the system which is defined as

$$C_{i,j} = \langle a_i^\dagger a_j \rangle. \quad (55)$$

The equations of motion are given by

$$\begin{aligned} \frac{dC_{i,j}}{dt} = & i g (C_{i-1,j} - C_{i,j+1} + C_{i+1,j} - C_{i,j-1}) \\ & - (\Gamma_L \mp \Gamma_G) (\delta_{im} + \delta_{jm}) C_{i,j} + 2 \Gamma_G \delta_{mi} \delta_{mj}, \end{aligned} \quad (56)$$

where \mp stands for bosons and fermions, respectively. It is crucial to note that Γ_G [Eq. (53)] and Γ_L [Eq. (54)] here are related by detailed balance, i.e., they are not independent of each other.

We now solve for correlation functions in Eq. (56) and subsequently extract the local population and total occupation. Without loss of generality, in this subsection, we consider the bath to be attached to the lattice at site $m = 0$. Furthermore, we take the lattice size L to be infinity, i.e., the lattice is now extended from $-\infty$ to $+\infty$. Since the system is expected to be symmetric about the 0th site, for simplicity, we consider only the positive side of the lattice chain in the analysis presented below. The spatial density profile $n_i(t)$ is given by (see the Appendix for the details)

$$n_i(t) = 2 \Gamma_G \int_0^t d\tau |\tilde{\mathcal{S}}_i(\tau)|^2, \quad (57)$$

where for large τ ,

$$\tilde{\mathcal{S}}_i(\tau) = \frac{i J_i(2g\tau)}{i + \tau \Gamma'}. \quad (58)$$

Here J_i is the Bessel function of the first kind and

$$\Gamma' = \Gamma_L \mp \Gamma_G = \frac{J(0)}{2}, \quad (59)$$

where \mp stands for bosons and fermions, respectively, and we recall that Γ_G and Γ_L are given in Eqs. (53) and (54), respectively. Interestingly, Γ' defined in Eq. (59) is independent of the statistics and is always positive. As a consequence, the quantum statistics is encoded as a prefactor (Γ_G) in the density profile.

Interestingly, in the limit $i \rightarrow \infty$, $t \rightarrow \infty$ while keeping i/t as fixed, the analytical results in Eqs. (57) and (58) admit an interesting scaling form (see the Appendix for details)

$$n_i(t) = \Phi\left(\frac{i}{2gt}\right), \quad (60)$$

where the scaling function $\Phi(v)$ is exactly given by

$$\Phi(v) = \frac{4\Gamma_G g}{\pi} \int_1^{\frac{1}{v}} dz \frac{1}{\sqrt{z^2-1}} \frac{1}{(2g+z\Gamma')^2}. \quad (61)$$

The integral representation in Eq. (61) is identical (after a suitable change of variables) to Eq. (31) in Ref. [17] in which the dual problem of particle loss was studied. The integral in Eq. (61) can be performed exactly to yield

$$\Phi(v) = \frac{\Gamma_G \tilde{g}(1+\nu\tilde{g})[\ln(1+\nu\tilde{g}) - \ln(\tilde{g}+\nu - \sqrt{(\tilde{g}^2-1)(1-\nu^2)})] - \sqrt{(\tilde{g}^2-1)(1-\nu^2)}}{\Gamma' (\tilde{g}^2-1)^{3/2}(\nu\tilde{g}+1)}, \quad 0 < \nu < 1. \quad (62)$$

where the dimensionless parameters \tilde{g} are given by

$$\tilde{g} = \frac{2g}{\Gamma'} = \frac{4g}{J(0)} \quad (63)$$

and we recall that Γ' is given by Eq. (59) and $J(0)$ from Eq. (89) is given by

$$J(0) = \frac{2\gamma^2}{t_B}. \quad (64)$$

Note that the scaling function $\Phi(v)$ in Eq. (62) admits the following limiting forms near $\nu \rightarrow 0$ and $\nu \rightarrow 1$:

$$\Phi(v) = \frac{1}{1-\tilde{g}^2} - \frac{\tilde{g} \ln(\tilde{g} - \sqrt{\tilde{g}^2-1})}{(\tilde{g}^2-1)^{3/2}} - \frac{\nu^2}{2} + O(\nu^3) \quad (65)$$

when $\nu \ll 1$. Therefore, the decay of $\Phi(v)$ from the peak at $\nu = 0$ is parabolic in nature. This particular limit of $\nu = 0$ represents the property of the density profile in the bulk of the lattice. The two constant terms in Eq. (65) correspond to the locally thermalized value of the density in the vicinity of the injection site. On the other hand, the limit $\nu \rightarrow 1$ represents the density profile in the vicinity of the edge and we get

$$\Phi(v) = \frac{\sqrt{2(1-\nu)}}{1+\tilde{g}^2} + O[(1-\nu)^{3/2}] \quad \text{as } \nu \rightarrow 1. \quad (66)$$

From Eq. (66), it is interesting to note that the scaled density $\Phi(v)$ vanishes in a square-root form. It is worth noting that the analytical scaling form in Eq. (61) is independent of quantum statistics except the prefactor (Γ_G).

The total particle number $N(t)$ is given by (see Appendix for details)

$$\begin{aligned} N(t) &= \frac{4\Gamma_G \tilde{g}^2 t}{\pi} \int_1^\infty \frac{dz}{z} \frac{1}{\sqrt{z^2-1}} \frac{1}{(\tilde{g}+z)^2} \\ &= -\frac{2\Gamma_G t}{\pi(1-\tilde{g}^2)} \left[2\tilde{g} - \pi(1-\tilde{g}^2) + 2(1-2\tilde{g}^2) \frac{\cos^{-1}(\tilde{g})}{\sqrt{1-\tilde{g}^2}} \right]. \end{aligned} \quad (67)$$

Note that using the relation

$$\frac{\cos^{-1}(\tilde{g})}{\sqrt{1-\tilde{g}^2}} = -\frac{\ln(\tilde{g} + \sqrt{\tilde{g}^2-1})}{\sqrt{\tilde{g}^2-1}} \quad (68)$$

it is easy to see that Eq. (67) is always real for all values of \tilde{g} . From Eq. (67) it is clear that $N(t)$ always exhibits a linear growth in time. One can further simplify Eq. (67) in the limit of small and large \tilde{g} . We get

$$N(t) = t\Gamma_G \left[\tilde{g}^2 - \frac{16}{3\pi} \tilde{g}^3 \right] + O(\tilde{g}^4) \quad (69)$$

when $\tilde{g} \ll 1$ and

$$N(t) = t\Gamma_G \left[2 + \frac{4}{\pi} \frac{1 - \ln(4) - 2 \ln(\tilde{g})}{\tilde{g}} \right] + O\left(\frac{1}{\tilde{g}^3}\right), \quad (70)$$

when $\tilde{g} \gg 1$.

Note that although the Redfield (Sec. II B) and Lindblad (Sec. II C) equations offer us the advantage of tracking both time dynamics and steady state, it involves perturbative and Markovian approximations. To get an analytical handle of the steady state, via a fully nonperturbative approach, we now discuss the exact steady state using the quantum Langevin approach.

D. Method 4: Quantum Langevin equation approach

In this subsection, we discuss the quantum Langevin equation (QLE) approach [36–44]. Given the bilinear nature of the entire setup, we can compute exactly the steady-state properties of the lattice chain following this approach. Let us start by rewriting the Hamiltonian in Eqs. (1)–(3) as

$$\begin{aligned} H_S &= \sum_{i,j=1}^L h_{ij}^S a_i^\dagger a_j, & H_B &= \sum_{i,j=1}^{L_B} h_{ij}^B b_i^\dagger b_j, \\ H_{SB} &= \sum_{i=1}^L \sum_{j=1}^{L_B} h_{ij}^{SB} a_i^\dagger b_j + \text{H.c.} \end{aligned} \quad (71)$$

Let us denote $A(t) = \{a_i(t)\}$ and $B(t) = \{b_i(t)\}$ as the column vectors consisting of system and bath annihilation operators,

respectively. The Heisenberg equations of motion for the respective components are given as

$$\dot{A}(t) = -ih^S A(t) - ih^{SB} B(t), \quad (72)$$

$$\dot{B}(t) = -ih^B B(t) - ih^{SB\dagger} A(t). \quad (73)$$

We first solve the bath equations in Eq. (73) and then substitute the solution to the system's equation of motion in Eq. (72). The formal solution of Eq. (73) is given by

$$b_i(t) = i \sum_{r=1}^{L_B} [g^+(t-t_0)]_{ir} b_r(t_0) + \int_{t_0}^{\infty} d\tau \sum_{r=1}^{L_B} \sum_{s=1}^L [g^+(t-\tau)]_{ir} h_{rs}^{SB\dagger} a_s(\tau), \quad (74)$$

where $i = 1, 2, \dots, L_B$ denotes the indices for bath operators. The Green's function

$$g^+(t) = -i\theta(t) e^{-ih^B t} \quad (75)$$

$$\langle \eta_i^\dagger(t) \eta_j(t') \rangle = \sum_{r,r'=1}^{L_B} h_{ir}^{SB*} \left(\sum_{q=1}^{L_B} U_{rq}^* U_{r'q} \bar{n}(\lambda_q^B) e^{i\lambda_q^B(t-t')} \right) h_{r'j}^{SB\dagger} \theta(t-t_0) \theta(t'-t_0), \quad (79)$$

where recall that the matrix U is responsible for diagonalizing the single-particle Hamiltonian h^B of the bath [see Eq. (18)]. Since we are interested in the steady-state limit, we first take $L_B \rightarrow \infty$ and then let $t_0 \rightarrow -\infty$. As a result, $\theta(t-t_0)$ and $\theta(t'-t_0)$ in Eq. (79) are always equal to unity. Let us now define Fourier transformation of $\eta_i(t)$ as

$$\tilde{\eta}_i(\omega) = \int_{-\infty}^{\infty} dt e^{i\omega t} \eta_i(t) \quad (80)$$

and the corresponding inverse is given as

$$\eta_i(t) = \int_{-\infty}^{\infty} \frac{d\omega}{2\pi} e^{-i\omega t} \tilde{\eta}_i(\omega). \quad (81)$$

Using Eqs. (80) and (79), we get

$$\langle \tilde{\eta}_i^\dagger(\omega) \tilde{\eta}_j(\omega') \rangle = 4\pi^2 \Gamma_{ji}(\omega) \bar{n}(\omega) \delta(\omega - \omega'), \quad (82)$$

where

$$\Gamma_{ji}(\omega) = \sum_{r,r'=1}^{\infty} h_{jr'}^{SB} \rho_{r'r}(\omega) h_{ri}^{SB\dagger}, \quad (83)$$

$$\rho_{r'r}(\omega) = \sum_{q=1}^{\infty} U_{rq}^* U_{r'q} \delta(\omega - \lambda_q^B).$$

We obtain the solution of Eq. (76) in the Fourier space as

$$\tilde{a}_i(\omega) = \sum_{s=1}^L G_{is}^+(\omega) \tilde{\eta}_s(\omega), \quad (84)$$

where $\tilde{a}_i(\omega)$ is the Fourier transformation of $a_i(t)$ with definition same as Eq. (80). The retarded Green's function $G^+(\omega)$

is the solution of the homogeneous part of Eq. (73) and $\theta(t)$ is the Heaviside step function. Substituting this solution in Eq. (72), we obtain the quantum Langevin equation (QLE) for the system operators as

$$\dot{a}_i(t) = -i \sum_{s=1}^L h_{is}^S a_s(t) - i \eta_i(t) - i \int_{t_0}^{\infty} d\tau \sum_{s=1}^L \Sigma_{is}^+(t-\tau) a_s(\tau). \quad (76)$$

Note that, in Eq. (76), the effect of the bath appears as a self-energy and a noise term, which are given, respectively, as

$$\Sigma^+(t-\tau) = h^{SB} [g^+(t-\tau)] h^{SB\dagger}, \quad (77)$$

$$\eta(t) = i h^{SB} [g^+(t-t_0)] B(t_0). \quad (78)$$

The statistical property of the noise operator gets determined by the initial condition of the bath density operator, as given in Eq. (5). As a result, $\langle \eta_i(t) \rangle = 0$. The noise correlation at different times can be expressed in terms of the normal modes of the bath as

that appears in Eq. (84) is given as

$$G^+(\omega) = [\omega I - h^S - \Sigma^+(\omega)]^{-1}, \quad (85)$$

where $\Sigma^+(\omega)$ is now the self-energy matrix in the Fourier space and is defined as

$$\Sigma^+(\omega) = h^{SB} \tilde{g}^+(\omega) h^{SB\dagger}. \quad (86)$$

Here, $\tilde{g}^+(\omega)$ is the Fourier transform of $g^+(t)$ [see Eq. (75)] and is given as

$$[\tilde{g}^+(\omega)]_{rr'} = \sum_{q=1}^{\infty} \frac{U_{rq} U_{r'q}^*}{\omega - \lambda_q^B + i0^+}, \quad (87)$$

where the small imaginary component appears to preserve the causality of $g^+(t)$. Finally, using Eq. (84) and the noise-noise correlation in Eq. (82), we obtain the spatial local density in the steady state as

$$n_i(t) = \langle a_i^\dagger(t) a_i(t) \rangle = \int_{-\infty}^{\infty} d\omega [G^+(\omega) \Gamma(\omega) G^-(\omega)]_{ii} \bar{n}(\omega), \quad (88)$$

where we recall that $\bar{n}(\omega)$ is either the Bose or the Fermi function as defined in Eq. (19). The integral in Eq. (88) can be performed numerically and the steady-state occupation at each site can be determined exactly. Note that the total occupation in the steady state can be obtained by following Eq. (7).

Having described the four methods in Secs. II A, II B, II C, and II D we now present our numerical findings using these methods.

III. NUMERICAL RESULTS FOR BOSONS

In this section, we present our numerical results for a one-dimensional nearest-neighbor tight-binding lattice which is coupled to an equilibrium bath at a particular site (recall Fig. 1). The quantities of interest are (i) local occupation number $n_i(t)$ versus i at fixed-time snapshots and (ii) the total occupation $N(t)$ versus t . We will mainly focus on presenting results for the bosonic case. We will briefly discuss the fermionic case and highlight interesting similarities and differences between the two in Sec. IV.

Unless otherwise stated, we choose the following parameters for the simulations. For the bath, we fix the parameters as intersite hopping $t_B = 1$, chemical potential $\mu = -2.01$, and inverse temperature $\beta = 1$. For the direct numerics, discussed in Sec. II A, we always choose $L_B = 4096$. We connect the bath at a particular site m of the lattice. For the Redfield (Sec. II B), Lindblad (Sec. II C), and quantum Langevin (Sec. II D) equation approaches, the bath is considered to be a semi-infinite one-dimensional tight-binding chain, and the corresponding form of the spectral density $J(\omega)$ can be obtained exactly, given as [27]

$$J(\omega) = \frac{2\gamma^2}{t_B} \sqrt{1 - \frac{\omega^2}{4t_B^2}}. \quad (89)$$

Before proceeding further, we note that depending on the method employed and specific quantities of interests, the system size L , hopping parameter g , and the system-bath coupling γ are chosen by taking into account computational feasibility and better clarity of presentation.

A. Nonperturbative regime in system-bath coupling

In Fig. 2 we show the total occupation $N(t)$ as a function of time t using the direct exact numerics, described in Sec. II A. The early-time linear behavior and long-time exponential relaxation towards the steady state are clearly seen. We also present the steady-state value obtained from the quantum Langevin equation approach, described in Sec. II D, and observe that the long-time limit for $N(t)$ from direct exact numerics approaches to the exact steady-state value. Notice that we clearly observe an exponential relaxation of $N(t)$ towards the steady state (see inset of Fig. 2). This is consistent with the relaxation dynamics of finite-size systems coupled to a generic bath. This exponential relaxation can, in fact, be rigorously established following the Redfield approach (Sec. II B). $N(t)$ reaching a steady-state value is a result of finite system size which here is taken to be $L = 40$. Also, to ensure that the steady-state value is reached relatively fast, we choose $\gamma = 1$ which falls into the nonperturbative regime of the system-bath coupling. We expect that the time to reach steady state t_{SS} increases with system size L . By performing direct exact numerics we find that the times to reach steady state for $L = 16, 20$, and 40 are $t_{SS} \sim 175, 330$, and 2000 , respectively. Based on these numbers, we find that the dependence of t_{SS} on system size L is $t_{SS} \sim L^\delta$ where $\delta \approx 2.5$. In the large- L limit one would expect the scaling to go as $t_{SS} \sim L^2$ which is related to the fact that the adjacent energy gaps in a tight-binding chain scale as $1/L^2$.

One would expect $N(t)$ to grow linearly for an infinite lattice. To demonstrate this, using direct numerics (Sec. II A), we show in Fig. 3 the behavior of $N(t)$ versus t for different system sizes. It can be noticed that the deviation from the linear growth starts at a timescale that scales with the system size L .

In Fig. 4, we show the spatial density profile $n_i(t)$ [Eq. (6)] as a function of lattice coordinate i for various time snapshots t using direct numerics (Sec. II A). The long-time limit of this density profile agrees perfectly with that obtained using the quantum Langevin equation approach, described in Sec. II D. Note that here we choose the lattice size $L = 20$ and the bath is connected to the lattice at site $m = 11$. Therefore, this particular site shows maximum average local occupation and eventually thermalizes with the bath, thereby settling to a finite value. The nearby sites gradually develop local occupation and finally settle down to a finite value, owing to indirect thermalization with the bath. In the long-time limit, an interesting pattern of local density profile is formed. At very large times, the relatively flat pattern of the local density profile, away from the center, is an interesting observation. Note that apart from the system size the parameters chosen in Fig. 4 are exactly the same as in Figs. 2 and 3 and therefore we remain in the nonperturbative system-bath coupling regime. We choose system size $L = 20$ keeping in mind computational feasibility and to ensure a relatively quick approach to steady state.

In Fig. 5 we present a zoomed view of the spread of local density profiles $n_i(t)$ for $L = 100$ sites with bath connected at $m = 51$, for different time snapshots. The ballistic spread of the density profile with velocity $2g$ can be clearly seen, where we recall that g is the intersite hopping within the lattice system. This indicates a scaling form for the profile which is presented in Fig. 6. Note that the parameters chosen in Figs. 5 and 6 are exactly the same as in Figs. 2–4 except the value of g which is chosen to be 0.25 in order to illustrate ballistic spreading over a computationally feasible system size L .

B. Perturbative regime in system-bath coupling

Next, we discuss the regime of weak system-bath coupling which further allows us to employ the Redfield (Sec. II B) and Lindblad (Sec. II C) approaches. Unlike Figs. 2–4 where we had set $\gamma = 1$, in Fig. 7 we choose $\gamma = 0.01$ to ensure that we remain in weak system-bath (perturbative) coupling regime. We retain the value of $g = 0.5$ as before which therefore does not fall in the validity of local Lindblad equation approach, as was also mentioned in Sec. II C. In Fig. 7 we first compare the local density profile $n_i(t)$ obtained following direct exact numerics, discussed in Sec. II A and the Redfield approach, discussed in Sec. II B. We observe perfect agreement at various time snapshots. Moreover, the inset in Fig. 7 also shows excellent agreement between the two approaches for the total occupation $N(t)$ [Eq. (7)]. The slope obtained from this inset plot perfectly matches with the slope extracted following the short-time (relative to the time to reach the steady state) dynamics described by Eq. (47). Note that as a consequence of lower value of system-bath coupling γ , the time required to reach steady state is very long and much higher than the time snapshots presented in Fig. 7. This further implies that the

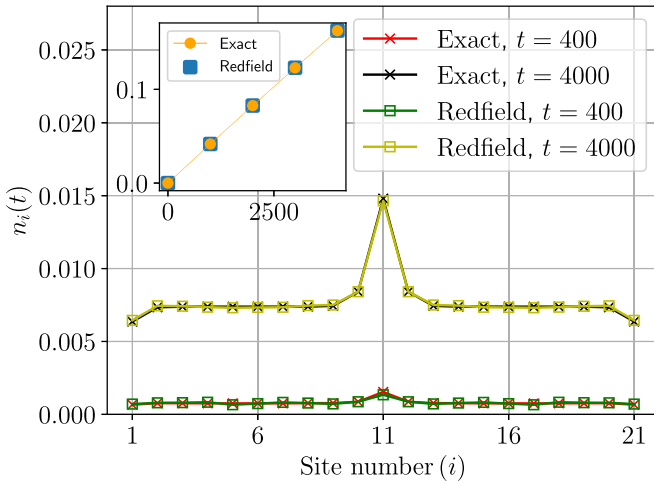


FIG. 7. Local density profile $n_i(t)$ [Eq. (6)] for bosons with $L = 21$ lattice sites with bath attached at a particular site ($m = 11$) for various time snapshots ($t = 400$, $t = 4000$) using direct exact numerics (cross), as discussed in Sec. II A. We show good agreement of these results with that obtained using the Redfield equation approach (squares), discussed in Sec. II B. The inset shows total occupation $N(t)$ [Eq. (7)] for $t = 1000, 2000, 3000, 4000$ with both direct exact numerics (Sec. II A) and Redfield (Sec. II B) approaches. The slope obtained from this plot perfectly matches with the slope extracted following Eq. (47). The parameters are $t_B = 1$, $g = 0.5$, $\beta = 1$, $\mu = -2.01$, and $\gamma = 0.01$. Note that as $\gamma = 0.01$ and $g = 0.5$, the Redfield approach is well suited for comparison with the direct exact numerics. Also, as a consequence of low value of γ , the time to reach steady state is very long and much higher than the times presented in this figure. This further implies that the steady value of local density is far from the values presented here.

steady value of local density is far from the values presented in Fig. 7. For the same parameter values as in Fig. 7, we show the results for total occupation $N(t)$ in Fig. 8 following the direct exact numerics, Redfield, and Lindblad approaches. We observe a perfect agreement between the exact numerics and the Redfield approach, whereas the result obtained from the Lindblad approach differs significantly due to the chosen relatively large- g value. Note that, for both large g and large γ , the Redfield approach shows an exponential growth in the total occupation number, as shown in Fig. 9, further indicating a complete breakdown of the perturbative approach. In Fig. 10 we show the results for $N(t)$ by reducing both the g value and the γ value and see an almost perfect agreement between all the three complementary methods. Our detailed analysis, therefore, provides guiding principles for the appropriate choice of parameters. In Figs. 11 and 12, we show the rate of early-time growth of the total occupation as a function of g and γ , respectively. In Figs. 13 and 14, we show the behavior of total occupation at steady state N_{SS} as a function of g and γ , respectively, for QLE, exact numerics, Redfield, and Lindblad approaches. Interestingly, in the regime when $\gamma \sim g$ (keeping both of them small), as seen in the first data point in Fig. 13, local Lindblad approach shows better agreement with exact and QLE than Redfield approach. This could be rooted in the fact that when $\gamma \gtrsim g$ (still keeping both of them small), the resulting dynamics is

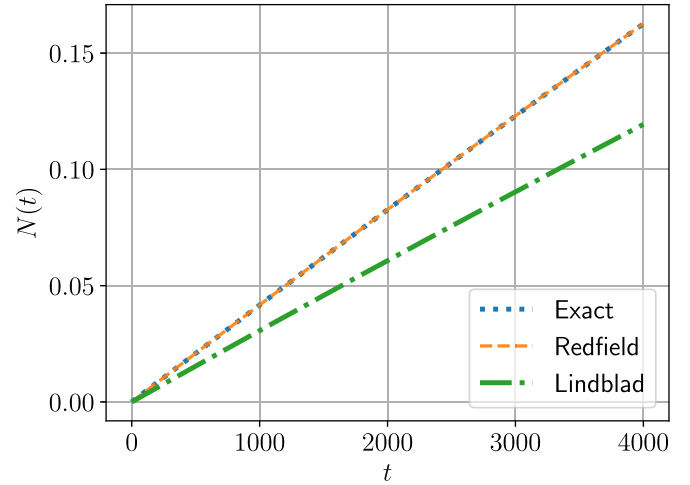


FIG. 8. Behavior of total occupation $N(t)$ [Eq. (7)] versus t for system size $L = 21$ for the bosonic case, comparing direct exact numerics, Redfield, and Lindblad approaches. The bath is connected at site number $m = 11$. The parameters are $g = 0.5$, $\gamma = 0.01$, $t_B = 1$, $\beta = 1$, and $\mu = -2.01$. This plot shows that the Redfield approach agrees with exact numerics whereas the local Lindblad deviates. This is due to relatively large intersite hopping g .

such that the lattice site connected to the bath gets occupied while a small- g value disallows the spreading to other lattice sites. In such a scenario a local description of the open quantum system, such as the local Lindblad equation, could

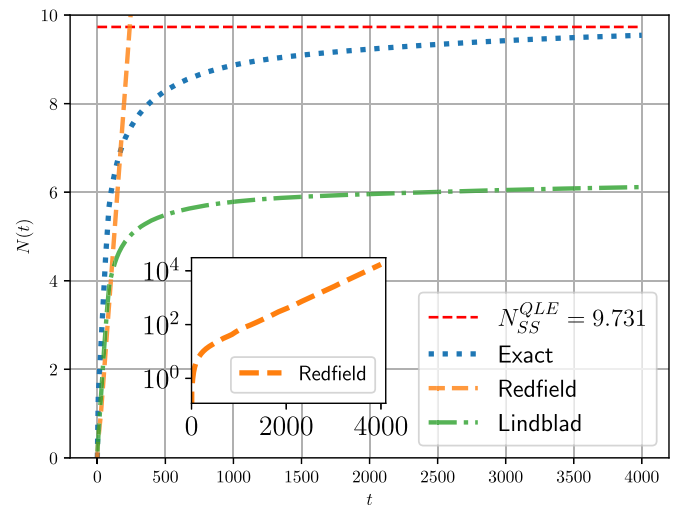


FIG. 9. Behavior of total occupation $N(t)$ [Eq. (7)] versus t for system size $L = 40$ for the bosonic case, comparing exact numerics, Redfield, and Lindblad approaches. This figure is analogous to Fig. 2 in the main text. The bath is connected at site number $m = 21$. The red dashed line shows the steady-state value N_{SS}^{QLE} obtained from the quantum Langevin equation approach. The parameters are $g = 0.5$, $\gamma = 1$, $t_B = 1$, $\beta = 1$, and $\mu = -2.01$. The inset shows the plot for total occupation $N(t)$ versus t for the Redfield approach demonstrating exponential growth of total occupation number. This plot shows that neither of the perturbative approaches agrees with exact numerics, implying the invalidity of these approaches in this parameter regime.

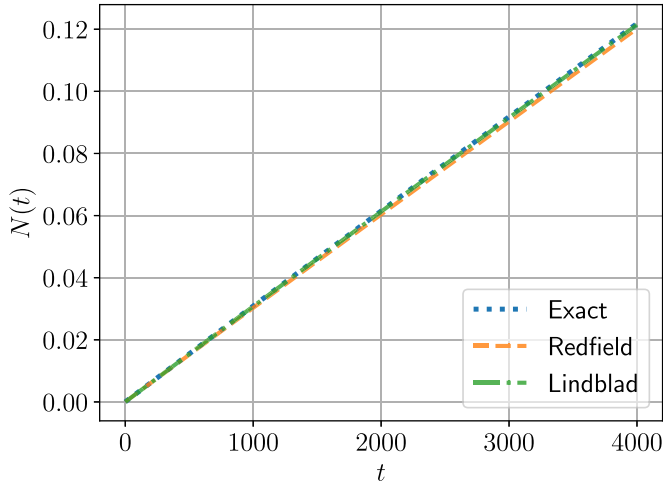


FIG. 10. Behavior of total occupation $N(t)$ [Eq. (7)] versus t for system size $L = 41$ for the bosonic case, comparing exact numerics, Redfield, and Lindblad approaches. The bath is connected at site number $m = 21$. The parameters are $g = 0.05$, $\gamma = 0.01$, $t_B = 1$, $\beta = 1$, and $\mu = -2.01$. This plot shows that both of the perturbative approaches agree well with exact numerics, implying the validity of these approaches in this parameter regime.

more appropriately describe the dynamics of the open system than a global master equation such as the Redfield equation. In Fig. 15 we plot the local density $n_i(t)$ for two different time snapshots and demonstrate excellent agreement between the analytical results given by Eqs. (57) and (58) with direct exact numerics (Sec. II A). The inset in Fig. 15 shows a plot for $N(t)$ vs t in the same parameter regime which shows a perfect linear growth with slope $2\Gamma_G$ and therefore matches with the prediction in Eq. (70) In Fig. 16 we use the same parameters as in Fig. 15 and demonstrate excellent agreement between the scaled version of data in Fig. 15, analytical scaling form (Sec. II C) given in Eq. (61).

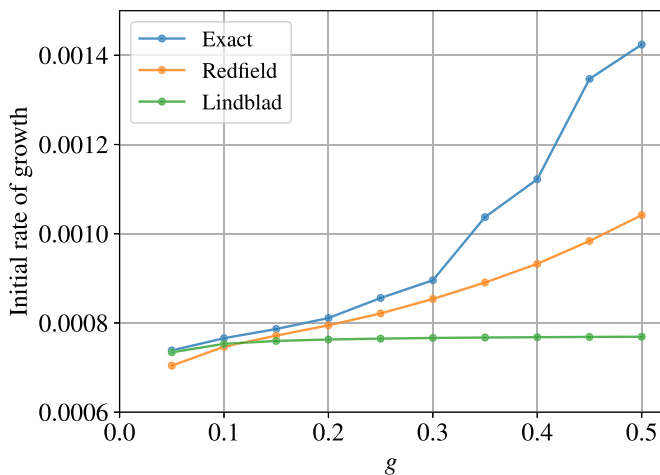


FIG. 11. Initial rate of growth of total occupation as a function of g , keeping γ fixed for system size $L = 5$ with bosons, comparing exact numerics, Redfield, and Lindblad approaches. The bath is connected at site number $m = 3$. The parameters are $\gamma = 0.05$, $t_B = 1$, $\beta = 1$, and $\mu = -2.01$.

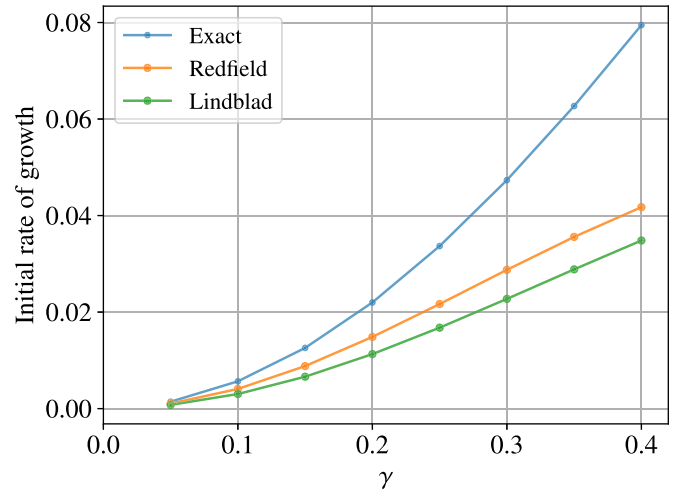


FIG. 12. Initial rate of growth of total occupation as a function of γ , keeping g fixed for system size $L = 5$ with bosons, comparing exact numerics, Redfield, and Lindblad approaches. The bath is connected at site number $m = 3$. The parameters are $g = 0.5$, $t_B = 1$, $\beta = 1$, and $\mu = -2.01$.

IV. NUMERICAL RESULTS FOR FERMIONS

So far we presented results for bosons. We now briefly make a few comments about fermions highlighting the similarities and differences. We find that owing to the Pauli exclusion principle, fermions experience blockade which makes its quantum dynamics different from that of bosons. The rate of growth of $N(t)$ at small times is higher for bosons as they are not limited by the Pauli exclusion principle obeyed by fermions. As a result of such slow growth for fermions, in the long-time limit overall total occupation $N(t)$ within the lattice is significantly lower in comparison with bosons. Similar to bosons, the fermions also exhibit overall

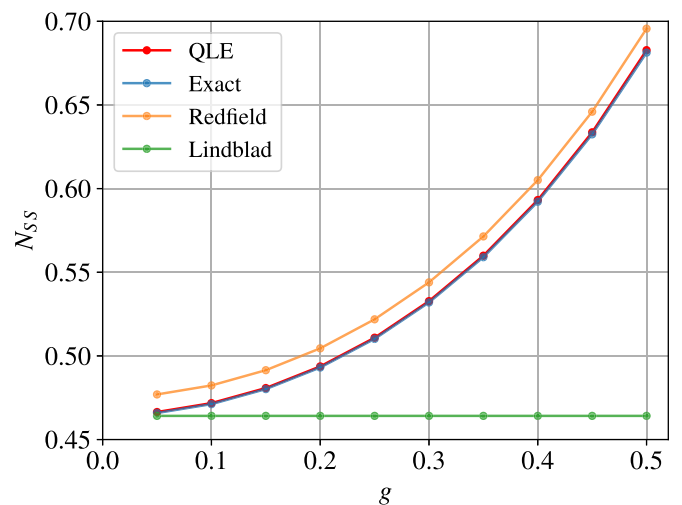


FIG. 13. Behavior of total occupation at steady state N_{SS} as a function of g , keeping γ fixed for system size $L = 5$ with bosons, comparing exact numerics, QLE, Redfield, and Lindblad approaches. The bath is connected at site number $m = 3$. The parameters are $\gamma = 0.05$, $t_B = 1$, $\beta = 1$, and $\mu = -2.01$.

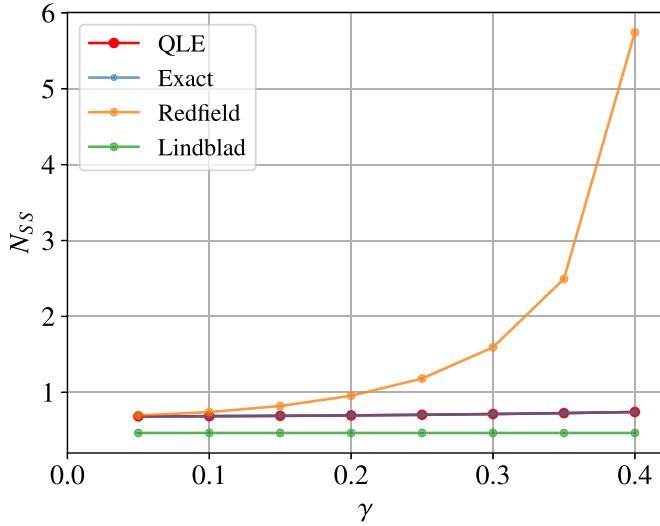


FIG. 14. Behavior of total occupation at steady state N_{SS} as a function of γ , keeping g fixed for system size $L = 5$ with bosons, comparing exact numerics, QLE, Redfield, and Lindblad approaches. The bath is connected at site number $m = 3$. The parameters are $g = 0.5$, $t_B = 1$, $\beta = 1$, and $\mu = -2.01$.

early-time linear growth and exponential relaxation at long times. In Fig. 17 we demonstrate these trends following the direct exact numerics described in Sec. II A. In Fig. 18 we plot the local density profile for fermions at different time

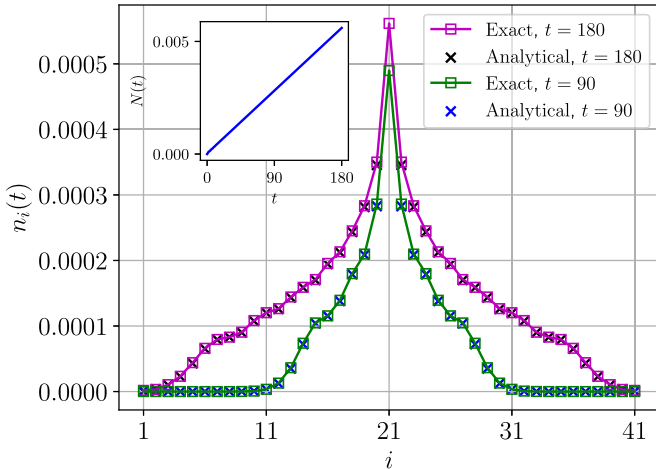


FIG. 15. Spatial density profile $n_i(t)$ [Eq. (6)] for bosons for $L = 41$ sites with the bath attached at $m = 21$ for two different time snapshots following direct exact numerics (Sec. II A), and analytical result based on Lindblad approach [Eqs. (57) and (58)] discussed in Sec. II C. We notice excellent agreement between the two approaches. The parameters chosen are $t_B = 1$, $g = 0.05$, $\beta = 1$, $\mu = -2.01$, and $\gamma = 0.01$. The plots are shown for time snapshot $t = 90$ and 180. Note that for the analytical case, no data are presented at $m = 21$ as the analytical expression in Eq. (58) is expected to only hold away from the lattice site where the bath is attached. Recall that we have chosen weak intersite hopping g to ensure the validity of local Lindblad approach. The inset shows the plot for total occupation $N(t)$ vs t for the same parameter values. The slope in the inset precisely turns out to be $2\Gamma_G$ and therefore matches with the prediction in Eq. (70) (Sec. II C).

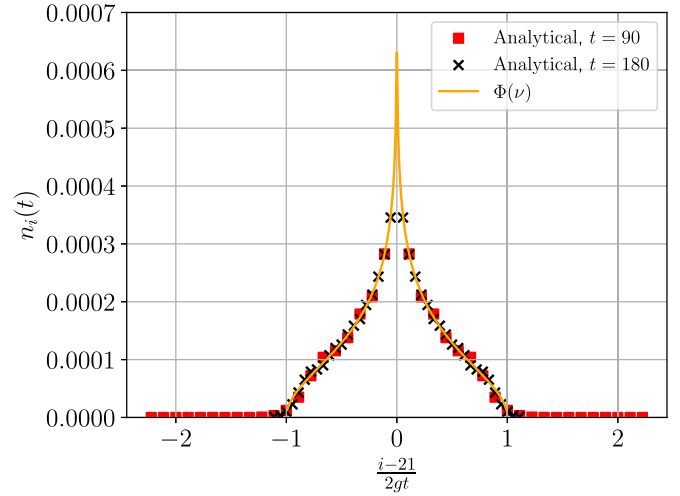


FIG. 16. Spatial scaled density profile $n_i(t)$ [Eq. (6)] for bosons for $L = 41$ sites with the bath attached at $m = 21$ for two different time snapshots following analytical result based on Lindblad approach (57) and (58) and the scaling form (61) discussed in Sec. II C. We notice excellent agreement between the two results. The parameters chosen are exactly the same as those of Fig. 15, i.e., $t_B = 1$, $g = 0.05$, $\beta = 1$, $\mu = -2.01$, and $\gamma = 0.01$. The plots are shown for time snapshot $t = 90$ and 180. Recall that we have chosen weak intersite hopping g to ensure the validity of the Lindblad approach.

snapshots following direct exact numerics and a relatively lower value in population compared to bosons is clearly observed, owing to the Pauli exclusion principle. In Fig. 19 we

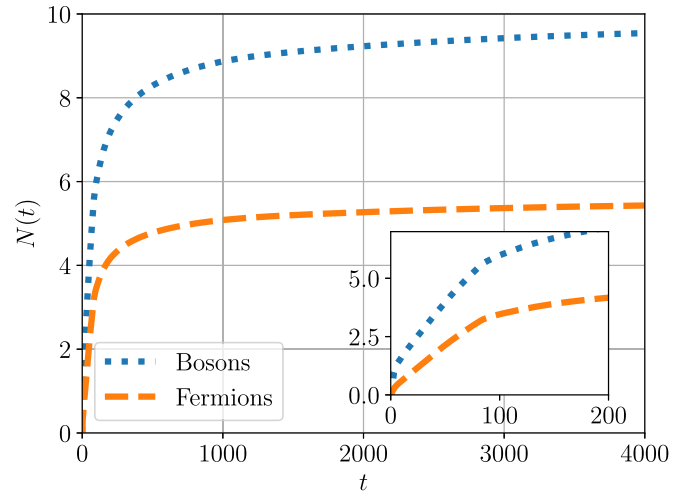


FIG. 17. Comparison between fermions and bosons for total occupation $N(t)$ for $L = 40$ sites with bath attached at $m = 21$, following direct exact numerics discussed in Sec. II A. It is clear from the plot that the eventual saturation value for fermions is smaller than that of bosons. The inset denotes the zoomed version of the dynamics at relatively short times and clearly shows that the rate of growth for the fermionic case is smaller than that of the bosonic case. The parameters chosen are $t_B = 1$, $g = 0.5$, $\beta = 1$, $\mu = -2.01$, and $\gamma = 1$. Note that although we have presented the results only from direct exact numerics Sec. II A, similar trends can be obtained following other methods.

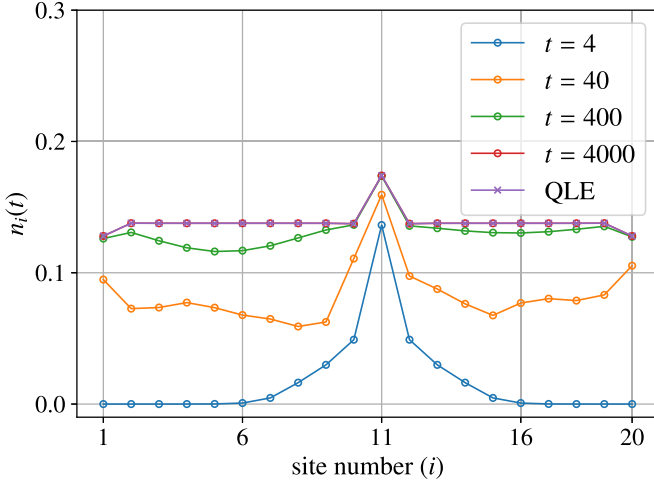


FIG. 18. Local density profile $n_i(t)$ [Eq. (6)] for fermions for $L = 20$ lattice sites with bath attached at a particular site ($m = 11$) for various time snapshots, using direct numerics (empty circles), as discussed in Sec. II A. The long-time limit of this density profile agrees perfectly with that obtained from QLE (cross), as discussed in Sec. II D. The parameters are $t_B = 1$, $g = 0.5$, $\beta = 1$, $\mu = -2.01$, and $\gamma = 1$. Note that the parameters chosen here are exactly the same as in Fig. 4.

show the ballistic growth of the density profile for fermions, similar to the bosonic case, following direct exact numerics. Interestingly, we observe a scaling trend for fermions in Fig. 20 similar to that of bosons. In suitable parameter regimes one can employ the other methods (Secs. II B, II C, II D) for fermions and notice similar trends.

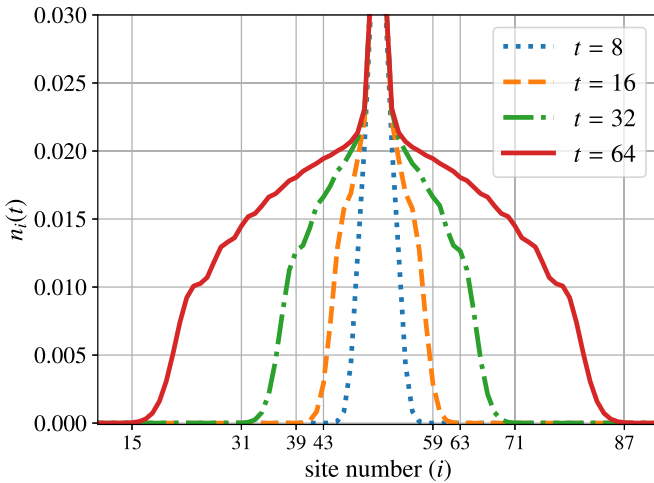


FIG. 19. Local density profile $n_i(t)$ [Eq. (6)] for fermions for $L = 100$ sites with bath attached at $m = 51$ from direct exact numerics, described in Sec. II A. We choose relatively short times to clearly demonstrate the ballistic growth of the density profile. We truncate the y axis to highlight the propagation of the density front. Note that this front of the density profiles spreads with velocity $c = 2g$, where g is the intersite hopping within the lattice. This figure clearly indicates the presence of scaling which is demonstrated in Fig. 6. The parameters are $t_B = 1$, $g = 0.25$, $\beta = 1$, $\mu = -2.01$, and $\gamma = 1$.

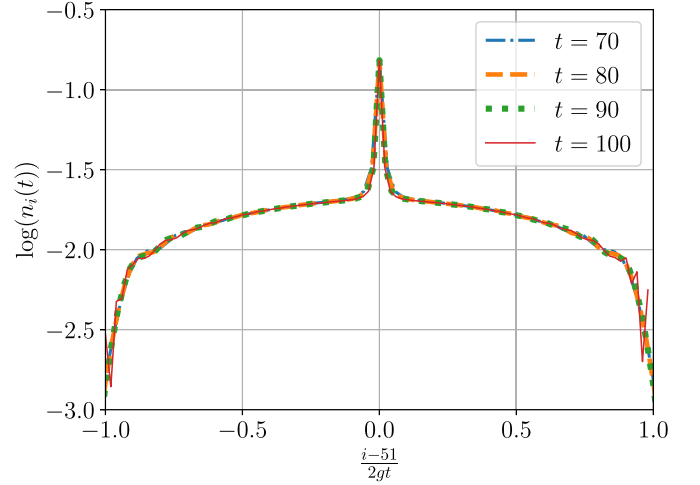


FIG. 20. A scaled plot of $\ln(n_i(t))$ [Eq. (6)] for fermions with $L = 100$ sites with bath attached at $m = 51$ to demonstrate the ballistic spread of spatial density profile $n_i(t)$ [Eq. (6)]. The parameters are $t_B = 1$, $g = 0.25$, $\beta = 1$, $\mu = -2.01$, and $\gamma = 1$. The logarithm mentioned in this plot is with base 10.

V. DISCUSSIONS AND COMPARISONS WITH PREVIOUS WORKS

As mentioned earlier, local gain or loss experienced by a system owing to a connection to a reservoir is an actively investigated area of research. Therefore, we place our work in the context of certain recent works. Note that, in our setup, the bath is responsible for simultaneous injection and/or removal of bosons or fermions with rates that obey a detailed balance condition. In other words, the rates of injection and removal are not arbitrary but are related. This condition is respected by all the methods (Sec. II) discussed in our work. If one considers only pure injection process (thereby not obeying detailed balance condition) both short- and long-time quantum dynamics can be drastically different [18,19]. For the case of bosons interesting dynamical transitions have been reported [19] when the system is subjected to an incoherent pump with no loss channels. More precisely, in the limit of large system sizes, $N(t)$ in Eq. (7) exhibits exponential or power-law growth depending on the incoherent pumping strength. However, an analogous setup for fermions [18] does not display such dynamical transitions and $N(t)$ grows linearly with t . This is an example where Pauli exclusion or lack thereof can have remarkably different consequences.

It is easy to note that if only incoherent pumping at a local site needs to be incorporated, then this amounts to artificially setting the loss coefficient $\Gamma_L = 0$ (thereby allowing the breakdown of detailed balance) in the Lindblad equation in Eq. (52). This results in the following equation of motion for the two-point correlation functions $C_{i,j}$ as defined in Eq. (55):

$$\begin{aligned} \frac{dC_{i,j}}{dt} = & i g (C_{i-1,j} - C_{i,j+1} + C_{i+1,j} - C_{i,j-1}) \\ & \pm \Gamma_G (\delta_{im} + \delta_{jm}) C_{i,j} + 2 \Gamma_G \delta_{mi} \delta_{mj}, \end{aligned} \quad (90)$$

where note the crucial sign difference in the second term with + sign indicates bosons and - sign indicates fermions. This

\pm sign in Eq. (90) arising due to quantum statistics leads to a crucial change in the dynamics for local density $n_i(t)$ in Eq. (6) and total occupation $N(t)$ in Eq. (7). More explicitly, following the differential equation in Eq. (90), one can show a linear growth for $N(t)$ versus t for fermions [18], whereas for bosons exponential and power-law growth in time can be seen [19].

It is important to note that if one has to respect the detailed balance condition, it is not possible to set Γ_L to 0. In fact, one can interestingly notice that from Eqs. (53) and (54) that for bosons, $\Gamma_L > \Gamma_G$ is always true. As a consequence, the term $-(\Gamma_L \mp \Gamma_G)(\delta_{im} + \delta_{jm})$ in Eq. (56) is always negative for bosons. The same is straightforward to notice even for the case of fermions. Therefore, for both bosons and fermions, Eq. (56) bears strong structural resemblance with the equation obtained when a fermionic lattice [corresponding to negative sign in the second term of Eq. (90)] is subjected only to incoherent pump [18] yielding Eq. (90). This argument explains why via the methods employed in this work we see linear growth in $N(t)$ irrespective of whether one considers bosons or fermions.

VI. SUMMARY AND OUTLOOK

In this work, we demonstrate how a complex interplay between unitary and nonunitary dynamics and quantum statistics can lead to nontrivial quantum dynamics and subsequent steady state. We considered the setup when an empty lattice is locally connected to a reservoir (Fig. 1). The main quantities of interest were local spatial density profile $n_i(t)$ [Eq. (6)] and the total occupation $N(t)$ [Eq. (7)]. We employed four methods: (i) direct exact numerics for correlation matrix (Sec. II A), (ii) Redfield equation (Sec. II B), (iii) Lindblad equation (Sec. II C), and (iv) exact quantum Langevin approach (Sec. II D).

We showed that the initial growth for the total occupation $N(t)$ for both bosons and fermions is linear in time and it subsequently saturates (for a finite lattice size) to a constant value in an exponential manner. For an infinite lattice, there is no saturation and $N(t)$ grows linearly with time. The local spatial density profile $n_i(t)$ exhibits a ballistic spatial spread for both bosons and fermions. At any fixed lattice coordinate, $n_i(t)$ initially grows in time and eventually saturates owing to equilibration with the bath. Our simulation results indicate that the equilibration time $t_{SS} \sim L^\delta$ with $\delta \approx 2.5$. However, we expect $\delta = 2$ in the large- L limit. Our work unravels the universal features and the differences between bosons and fermions the cause of which is rooted in quantum statistics. In the context of recent works on this subject, it is to be noted that our microscopic starting point is drastically different from phenomenological approaches [18,19]. We show that restoring detailed balance condition plays a pivotal role in deciding the fate of the quantum dynamics. We also show that our findings for spatial density profile obey analytical forms in an appropriate parameter regime.

Future work will be directed towards understanding quantum dynamics for filling particles in higher-dimensional lattices with arbitrary geometries and fully and partially connected networks [45–49]. Understanding the full counting

statistics [50] and distribution of total occupation, $P[N(t)]$, will be a problem of significant interest. A challenging and interesting question is understanding quantum dynamics and thermalization when reservoirs are locally connected to empty lattices that can host interacting bosons or fermions. It is important to highlight that with the current state-of-art experimental progress in absorption imaging techniques [51–53] and quantum gas microscopy [54–56], it has now become feasible to measure local density profiles for systems with very high precision even to the resolution at the level of a single atom.

ACKNOWLEDGMENTS

We thank K. Mallick for useful discussions. A.T. would like to thank the Long Term Visiting Students Program (LTVSP) of ICTS Bangalore. B.K.A. acknowledges the MATRICS grant (Grant No. MTR/2020/000472) from SERB, Government of India, and the Shastri Indo-Canadian Institute for providing financial support for this research work in the form of a Shastri Institutional Collaborative Research Grant (SICRG). B.K.A. would also like to acknowledge funding from the National Mission on Interdisciplinary Cyber-Physical Systems (NM-ICPS) of the Department of Science and Technology, Govt. of India, through the I-HUB Quantum Technology Foundation, Pune, India. M.K. would like to acknowledge support from the Project No. 6004-1 of the Indo-French Centre for the Promotion of Advanced Research (IFCPAR), Ramanujan Fellowship (Grant No. SB/S2/RJN-114/2016), SERB Early Career Research Award (Grant No. ECR/2018/002085), and SERB Matrics grant (Grant No. MTR/2019/001101) from the Science and Engineering Research Board (SERB), Department of Science and Technology (DST), Government of India. A.K. acknowledges the support of the core research Grant No. CRG/2021/002455 and the MATRICS Grant No. MTR/2021/000350 from the SERB, DST, Government of India. A.D., M.K., and A.K. acknowledge support of the Department of Atomic Energy, Government of India, under Project No. 19P1112R&D. This research was supported in part by the International Centre for Theoretical Sciences (ICTS) for participating in the program Physics with Trapped Atoms, Molecules and Ions (code: ICTS/TAMIONS-2022/5) and Bangalore School on Statistical Physics-XII (code: ICTS/bssp2021/6).

APPENDIX: ANALYTICAL FORMS FOR LOCAL DENSITY PROFILE $n_i(t)$ AND TOTAL OCCUPATION $N(t)$

In this Appendix, we present the details of the derivation of the analytical forms for local density profile $n_i(t)$ given in Eq. (57) and total occupation $N(t)$ given in Eq. (67). We start with the equations of motion for the correlation function [Eq. (55)] which we recall below:

$$\frac{dC_{i,j}}{dt} = i g (C_{i-1,j} - C_{i,j+1} + C_{i+1,j} - C_{i,j-1}) - (\Gamma_L \mp \Gamma_G)(\delta_{im} + \delta_{jm})C_{i,j} + 2\Gamma_G\delta_{mi}\delta_{mj}, \quad (\text{A1})$$

where \mp stands for bosons and fermions, respectively. Note that Γ_G is defined in Eq. (53) and Γ_L is defined in Eq. (54). We will closely follow Refs. [18,19] to derive the analytical

form for the density profile. For sake of brevity we define

$$\Gamma' = \Gamma_L \mp \Gamma_G, \quad (\text{A2})$$

where \mp stands for bosons and fermions, respectively. It is easy to see from Eqs. (53) and (54) that the following inequality holds for both bosons and fermions:

$$\Gamma' > 0. \quad (\text{A3})$$

Therefore, Eq. (A1) can be rewritten as

$$\begin{aligned} \frac{dC_{i,j}}{dt} = & i g (C_{i-1,j} - C_{i,j+1} + C_{i+1,j} - C_{i,j-1}) \\ & - \Gamma' (\delta_{im} + \delta_{jm}) C_{i,j} + 2 \Gamma_G \delta_{mi} \delta_{mj} \end{aligned} \quad (\text{A4})$$

with $\Gamma' > 0$ always. Note that Eq. (A4) is an inhomogeneous equation. Given that the lattice is initially in a vacuum, the following initial condition is satisfied:

$$C_{i,j}(t=0) = 0. \quad (\text{A5})$$

In order to solve Eq. (A4) along with the initial condition in Eq. (A5), we consider the following auxiliary problem. We will first solve Eq. (A4) without the inhomogeneous piece $2\Gamma_G \delta_{mi} \delta_{mj}$. Let us write the homogeneous equation as

$$\begin{aligned} \frac{d\tilde{C}_{i,j}}{d\tau} = & i g (\tilde{C}_{i-1,j} - \tilde{C}_{i,j+1} + \tilde{C}_{i+1,j} - \tilde{C}_{i,j-1}) \\ & - \Gamma' (\delta_{im} + \delta_{jm}) \tilde{C}_{i,j}, \end{aligned} \quad (\text{A6})$$

where the symbol tilde indicates an auxiliary function satisfying the homogeneous equation and we have used the symbol τ to differentiate the time variable with that of the actual problem. Closely following Refs. [18,19], we make the following ansatz:

$$\tilde{C}_{i,j}(\tau) = \tilde{S}_i(\tau) \tilde{S}_j^*(\tau). \quad (\text{A7})$$

Plugging in the ansatz given in Eq. (A7) into (A6), we can show that $\tilde{S}_i(\tau)$ satisfies the differential equation

$$\frac{d\tilde{S}_i}{d\tau} = i g [\tilde{S}_{i+1} + \tilde{S}_{i-1}] - \Gamma' \delta_{im} \tilde{S}_i, \quad (\text{A8})$$

where the time dependence τ on $\tilde{S}_i(\tau)$ in Eq. (A8) has been dropped for the sake of brevity.

One can show that solving the original inhomogeneous differential equation in Eq. (A4) along with the initial condition in Eq. (A5) can be achieved via solving the auxiliary homogeneous equation in Eq. (A6) with the initial condition

$$\tilde{C}_{i,j}(\tau=0) = \delta_{im} \delta_{jm}. \quad (\text{A9})$$

This auxiliary initial condition [Eq. (A9)] translates into

$$\tilde{S}_i(\tau=0) = \delta_{im}. \quad (\text{A10})$$

Without loss of generality, we henceforth consider the middle site to be at $m=0$. Furthermore, we take the lattice size L to be infinity, i.e., the lattice is now extended from $-\infty$ to $+\infty$. Since the system is expected to be symmetric about the 0th site, for simplicity, we consider only the positive side of the lattice chain in the analysis presented below. Now our goal

is to analyze Eq. (A8) along with the initial condition given by Eq. (A10). One can solve Eq. (A8) along with the initial condition (A10) using a combination of Laplace and Fourier transformations [18] and the solution is given as

$$\begin{aligned} \tilde{S}_i(\tau) = & J_i(2g\tau) - \Gamma' \int_0^\tau d\bar{\tau} e^{-\Gamma'\bar{\tau}} \\ & \times \left(\frac{\tau - \bar{\tau}}{\tau + \bar{\tau}} \right)^{i/2} J_i[2g\sqrt{\tau^2 - \bar{\tau}^2}], \end{aligned} \quad (\text{A11})$$

where $J_i(z)$ denotes the Bessel function of first kind. Note that the local density at a particular site i at time t is given as

$$n_i(t) = 2\Gamma_G \int_0^t d\tau |\tilde{S}_i(\tau)|^2. \quad (\text{A12})$$

Notice that in order to simplify Eq. (A12) one needs to use Eq. (A11) which itself has an integral, thereby making the simplification of $n_i(t)$ in Eq. (A12) complicated. Interestingly, it turns out that $n_i(t)$ can admit an interesting scaling form. To do so, let us take the limits

$$i \rightarrow \infty, \quad t \rightarrow \infty, \quad \nu = \frac{i}{2g\tau} \sim O(1), \quad (\text{A13})$$

where $\nu \sim O(1)$ is the scaled variable that will be used later. Owing to the scaling limit described in Eq. (A13), the upper limit of the integral can be set to infinity. Moreover, the contribution of the integral in Eq. (A12) largely comes when the integrand is evaluated at large τ . This can be checked numerically although it is not entirely obvious from Eq. (A11). Therefore, it is justified to simplify Eq. (A11) in the large- τ limit. In order to do so we use the following relation that holds for large τ :

$$\left(\frac{\tau - \bar{\tau}}{\tau + \bar{\tau}} \right)^{i/2} \approx e^{-i\frac{\bar{\tau}}{\tau}}. \quad (\text{A14})$$

Using Eq. (A14) in (A11) we obtain

$$\tilde{S}_i(\tau) = \frac{i J_i(2g\tau)}{i + \tau \Gamma'}. \quad (\text{A15})$$

Using the simplified form of $\tilde{S}_i(\tau)$ in Eq. (A15), the local density at a particular site is given as

$$n_i(t) = 2\Gamma_G \int_0^t d\tau |\tilde{S}_i(\tau)|^2 = 2\Gamma_G \int_0^t d\tau \frac{i^2 [J_i(2g\tau)]^2}{(i + \tau \Gamma')^2}, \quad (\text{A16})$$

where we recall that Γ_G is defined in Eq. (53) and $\tilde{S}_i(\tau)$ is given in Eq. (A15). Note that i in Eq. (A16) stands for lattice index. Equation (A16) is a compact analytical expression for the local density profile under the condition given in Eq. (A13). We now proceed to analytically derive the scaling form. To do so, we need to use the appropriate asymptotic expansion for the Bessel function that appears in Eq. (A16). Now

making a change of variable $\tau = t s$ and recalling $i = 2 g v t$, we rewrite Eq. (A16) as

$$n_i(t) = 8 \Gamma_G g^2 v^2 t \int_0^1 ds \frac{[J_{2gvt}(2 g t s)]^2}{(2 g v + s \Gamma')^2}. \quad (\text{A17})$$

To facilitate the implementation of the asymptotic form of Bessel function, it is convenient to introduce

$$\mu = 2 g v t \quad \text{and} \quad z = \frac{s}{v} \quad (\text{A18})$$

which simplifies Eq. (A17) as

$$n_i(t) = 8 \Gamma_G g^2 v t \int_0^{\frac{1}{v}} dz \frac{[J_\mu(\mu z)]^2}{(2 g + z \Gamma')^2}. \quad (\text{A19})$$

$$\zeta(z) = \begin{cases} \left(\frac{3}{2}\right)^{2/3} \left[\ln\left(\frac{\sqrt{z^2+1}+1}{z}\right) - \sqrt{1-z^2} \right]^{2/3} & \text{for } 0 < z \leq 1, \\ -\left(\frac{3}{2}\right)^{2/3} \left[\sqrt{z^2-1} - \sec^{-1}(z) \right]^{2/3} & \text{for } 1 < z \leq \infty. \end{cases} \quad (\text{A22})$$

We split Eq. (A19) as follows:

$$n_i(t) = 8 \Gamma_G g^2 v t \left[\int_0^1 dz \frac{[J_\mu(\mu z)]^2}{(2 g + z \Gamma')^2} + \int_1^{\frac{1}{v}} dz \frac{[J_\mu(\mu z)]^2}{(2 g + z \Gamma')^2} \right]. \quad (\text{A23})$$

To evaluate Eq. (A23) we use the appropriate forms in Eqs. (A20)–(A22) depending on the range of integration over z . It is easy to notice that the first integral in Eq. (A23) is exponentially suppressed in μ . Hence, keeping only the second term in Eq. (A23) and performing some manipulations, we get

$$n_i(t) = \frac{2 \Gamma_G g}{\pi} \int_1^{\frac{1}{v}} dz \frac{1}{\sqrt{z^2-1}} \frac{\mathcal{T}_\mu^2(\mu z)}{(2 g + z \Gamma')^2}. \quad (\text{A24})$$

$$\Phi(v) = \frac{\tilde{g}(1+v\tilde{g})[\ln(1+v\tilde{g}) - \ln(\tilde{g}+v - \sqrt{(\tilde{g}^2-1)(1-v^2)})] - \sqrt{(\tilde{g}^2-1)(1-v^2)}}{(\tilde{g}^2-1)^{3/2}(v\tilde{g}+1)}, \quad 0 < v < 1 \quad (\text{A27})$$

which is given in Eq. (62) of the main text. Here we introduced the dimensionless variable \tilde{g} as

$$\tilde{g} = \frac{2g}{\Gamma'} = \frac{4g}{J(0)}. \quad (\text{A28})$$

Our result in Eq. (A26) exactly coincides with the one obtained in Ref. [18] where a different approach was used. In a similar fashion, the total occupation number $N(t)$ is given by

$$\begin{aligned} N(t) &= \sum_{i=-\infty}^{\infty} n_i(t) = 4 g t \int_0^1 dv \Phi(v) \\ &= \frac{16 \Gamma_G g^2 t}{\pi} \int_0^1 dv \int_1^{\frac{1}{v}} dz \frac{1}{\sqrt{z^2-1}} \frac{1}{(2 g + z \Gamma')^2}. \end{aligned} \quad (\text{A29})$$

In the large- μ limit (for a fixed z) the asymptotic expansion of $J_\mu(\mu z)$ is given by [57,58]

$$J_\mu(\mu z) \sim \left(\frac{4 \zeta(z)}{1-z^2}\right)^{\frac{1}{4}} \frac{1}{2\sqrt{\mu\pi}} \frac{1}{|\zeta(z)|^{\frac{1}{4}}} \mathcal{T}_\mu(\mu z), \quad (\text{A20})$$

where $\mathcal{T}_\mu(\mu z)$ is given by

$$\mathcal{T}_\mu(\mu z) = \begin{cases} \exp\left[-\frac{2}{3}\mu\zeta(z)^{\frac{3}{2}}\right] & \text{for } 0 < z \leq 1, \\ 2 \cos\left[\frac{2}{3}\mu[-\zeta(z)]^{\frac{3}{2}} - \frac{\pi}{4}\right] & \text{for } 1 < z \leq \infty \end{cases} \quad (\text{A21})$$

with

We now use the expression for $\mathcal{T}_\mu(\mu z)$ from Eq. (A21) and get

$$n_i(t) = \frac{8 \Gamma_G g}{\pi} \int_1^{\frac{1}{v}} dz \frac{\cos^2\left[\frac{2}{3}\mu[-\zeta(z)]^{\frac{3}{2}} - \frac{\pi}{4}\right]}{(2 g + z \Gamma')^2 \sqrt{z^2-1}}. \quad (\text{A25})$$

For large μ , the cosine-squared term in the numerator is highly oscillatory and therefore can be approximated by $\frac{1}{2}$. We finally obtain the following scaling form for the local density profile $n_i(t)$:

$$\begin{aligned} n_i(t) &= \Phi\left(\frac{i}{2gt}\right), \quad \text{where} \\ \Phi(v) &= \frac{4 \Gamma_G g}{\pi} \int_1^{\frac{1}{v}} dz \frac{1}{\sqrt{z^2-1}} \frac{1}{(2 g + z \Gamma')^2} \end{aligned} \quad (\text{A26})$$

as also given in the main text in Eqs. (60) and (61). Upon performing the integral in Eq. (A26) we obtain

We next perform an integral by parts in Eq. (A29) which further simplifies $N(t)$ as

$$\begin{aligned} N(t) &= \frac{4 \Gamma_G \tilde{g}^2 t}{\pi} \int_1^\infty dz \frac{1}{z} \frac{1}{\sqrt{z^2-1}} \frac{1}{(\tilde{g}+z)^2} \\ &= -\frac{2 \Gamma_G t}{\pi(1-\tilde{g}^2)} \left[2\tilde{g} - \pi(1-\tilde{g}^2) \right. \\ &\quad \left. + 2(1-2\tilde{g}^2) \frac{\cos^{-1}(\tilde{g})}{\sqrt{1-\tilde{g}^2}} \right] \end{aligned} \quad (\text{A30})$$

which matches with the expression in Eq. (67) of the main text.

- [1] H.-P. Breuer and F. Petruccione, *The Theory of Open Quantum Systems* (Oxford University Press, Oxford, 2002).
- [2] H. J. Carmichael, *Statistical Methods in Quantum Optics 2: Non-classical Fields* (Springer, New York, 2009).
- [3] I. Rotter and J. Bird, A review of progress in the physics of open quantum systems: Theory and experiment, *Rep. Prog. Phys.* **78**, 114001 (2015).
- [4] A. Rivas and S. F. Huelga, *Open Quantum Systems* (Springer, Berlin, 2012), Vol. 10.
- [5] H.-P. Breuer, E.-M. Laine, J. Piilo, and B. Vacchini, Colloquium: Non-markovian dynamics in open quantum systems, *Rev. Mod. Phys.* **88**, 021002 (2016).
- [6] U. Weiss, *Quantum Dissipative Systems* (World Scientific, Singapore, 2012).
- [7] I. Reichental, A. Klemmner, Y. Kafri, and D. Podolsky, Thermalization in open quantum systems, *Phys. Rev. B* **97**, 134301 (2018).
- [8] M. Palmero, X. Xu, C. Guo, and D. Poletti, Thermalization with detailed-balanced two-site lindblad dissipators, *Phys. Rev. E* **100**, 022111 (2019).
- [9] H. Fröml, C. Muckel, C. Kollath, A. Chiocchetta, and S. Diehl, Ultracold quantum wires with localized losses: Many-body quantum zeno effect, *Phys. Rev. B* **101**, 144301 (2020).
- [10] P. Barmettler and C. Kollath, Controllable manipulation and detection of local densities and bipartite entanglement in a quantum gas by a dissipative defect, *Phys. Rev. A* **84**, 041606(R) (2011).
- [11] D. A. Zezyulin, V. V. Konotop, G. Barontini, and H. Ott, Macroscopic zeno effect and stationary flows in nonlinear waveguides with localized dissipation, *Phys. Rev. Lett.* **109**, 020405 (2012).
- [12] G. Kordas, S. Wimberger, and D. Witthaut, Decay and fragmentation in an open Bose-Hubbard chain, *Phys. Rev. A* **87**, 043618 (2013).
- [13] M. Kiefer-Emmanouilidis and J. Sirker, Current reversals and metastable states in the infinite Bose-Hubbard chain with local particle loss, *Phys. Rev. A* **96**, 063625 (2017).
- [14] D. Sels and E. Demler, Thermal radiation and dissipative phase transition in a bec with local loss, *Ann. Phys.* **412**, 168021 (2020).
- [15] R. Labouvie, B. Santra, S. Heun, and H. Ott, Bistability in a driven-dissipative superfluid, *Phys. Rev. Lett.* **116**, 235302 (2016).
- [16] Andreas Müllers, B. Santra, C. Baals, J. Jiang, J. Benary, R. Labouvie, D. A. Zezyulin, V. V. Konotop, and H. Ott, Coherent perfect absorption of nonlinear matter waves, *Sci. Adv.* **4**, eaat6539 (2018).
- [17] V. Alba and F. Carollo, Noninteracting fermionic systems with localized losses: Exact results in the hydrodynamic limit, *Phys. Rev. B* **105**, 054303 (2022).
- [18] P. Krapivsky, K. Mallick, and D. Sels, Free fermions with a localized source, *J. Stat. Mech.: Theory Exp.* (2019) 113108.
- [19] P. Krapivsky, K. Mallick, and D. Sels, Free bosons with a localized source, *J. Stat. Mech.: Theory Exp.* (2020) 063101.
- [20] M. Butz and H. Spohn, Dynamical phase transition for a quantum particle source, *Annales Henri Poincaré* (Springer, Berlin, 2010), Vol. 10, pp. 1223–1249.
- [21] P. Krapivsky, J. Luck, and K. Mallick, Survival of classical and quantum particles in the presence of traps, *J. Stat. Phys.* **154**, 1430 (2014).
- [22] A. Chakraborty and R. Sensarma, Power-law tails and non-markovian dynamics in open quantum systems: An exact solution from Keldysh field theory, *Phys. Rev. B* **97**, 104306 (2018).
- [23] P. L. Krapivsky, Symmetric exclusion process with a localized source, *Phys. Rev. E* **86**, 041103 (2012).
- [24] P. Krapivsky and D. Stefanovic, Lattice gases with a point source, *J. Stat. Mech.: Theory Exp.* (2014) P09003.
- [25] A. Sharma and E. Rabani, Landauer current and mutual information, *Phys. Rev. B* **91**, 085121 (2015).
- [26] J. M. Bhat and A. Dhar, Transport in spinless superconducting wires, *Phys. Rev. B* **102**, 224512 (2020).
- [27] A. Purkayastha, A. Dhar, and M. Kulkarni, Out-of-equilibrium open quantum systems: A comparison of approximate quantum master equation approaches with exact results, *Phys. Rev. A* **93**, 062114 (2016).
- [28] G. S. Agarwal, *Quantum Optics* (Cambridge University Press, Cambridge, 2012).
- [29] Z. Zhuang, J. Merino, and J. B. Marston, Transport in conductors and rectifiers: Mean-field redfield equations and nonequilibrium Green's functions, *Phys. Rev. B* **102**, 125147 (2020).
- [30] R. A. Pepino, J. Cooper, D. Meiser, D. Z. Anderson, and M. J. Holland, Open quantum systems approach to atomtronics, *Phys. Rev. A* **82**, 013640 (2010).
- [31] J. Wu, Non-equilibrium stationary states from the equation of motion of open systems, *New J. Phys.* **12**, 083042 (2010).
- [32] G. Lindblad, On the generators of quantum dynamical semigroups, *Commun. Math. Phys.* **48**, 119 (1976).
- [33] V. Gorini, A. Kossakowski, and E. C. G. Sudarshan, Completely positive dynamical semigroups of n-level systems, *J. Math. Phys.* **17**, 821 (1976).
- [34] D. Tupkary, A. Dhar, M. Kulkarni, and A. Purkayastha, Fundamental limitations in Lindblad descriptions of systems weakly coupled to baths, *Phys. Rev. A* **105**, 032208 (2022).
- [35] D. Manzano, A short introduction to the Lindblad master equation, *AIP Adv.* **10**, 025106 (2020).
- [36] A. Dhar and D. Sen, Nonequilibrium Green's function formalism and the problem of bound states, *Phys. Rev. B* **73**, 085119 (2006).
- [37] A. Dhar, K. Saito, and P. Hänggi, Nonequilibrium density-matrix description of steady-state quantum transport, *Phys. Rev. E* **85**, 011126 (2012).
- [38] A. Dhar and D. Roy, Heat transport in harmonic lattices, *J. Stat. Phys.* **125**, 801 (2006).
- [39] J.-S. Wang, X. Ni, and J.-W. Jiang, Molecular dynamics with quantum heat baths: Application to nanoribbons and nanotubes, *Phys. Rev. B* **80**, 224302 (2009).
- [40] G. W. Ford, J. T. Lewis, and R. F. O'Connell, Quantum Langevin equation, *Phys. Rev. A* **37**, 4419 (1988).
- [41] D. Segal, A. Nitzan, and P. Hänggi, Thermal conductance through molecular wires, *J. Chem. Phys.* **119**, 6840 (2003).
- [42] U. Zürcher and P. Talkner, Quantum-mechanical harmonic chain attached to heat baths. II. Nonequilibrium properties, *Phys. Rev. A* **42**, 3278 (1990).
- [43] Y.-C. Chen, J. L. Lebowitz, and C. Liverani, Dissipative quantum dynamics in a boson bath, *Phys. Rev. B* **40**, 4664 (1989).

- [44] N. Bondyopadhyaya and D. Roy, Nonequilibrium electrical, thermal and spin transport in open quantum systems of topological superconductors, semiconductors and metals, *J. Stat. Phys.* **187**, 11 (2022).
- [45] K. Wright, K. M. Beck, S. Debnath, J. Amini, Y. Nam, N. Grzesiak, J.-S. Chen, N. Pimenti, M. Chmielewski, C. Collins, *et al.*, Benchmarking an 11-qubit quantum computer, *Nat. Commun.* **10**, 5464 (2019).
- [46] K. Xu, Z.-H. Sun, W. Liu, Y.-R. Zhang, H. Li, H. Dong, W. Ren, P. Zhang, F. Nori, D. Zheng *et al.*, Probing dynamical phase transitions with a superconducting quantum simulator, *Sci. Adv.* **6**, eaba4935 (2020).
- [47] C. Song, K. Xu, H. Li, Y.-R. Zhang, X. Zhang, W. Liu, Q. Guo, Z. Wang, W. Ren, J. Hao *et al.*, Generation of multicomponent atomic Schrödinger cat states of up to 20 qubits, *Science* **365**, 574 (2019).
- [48] S. Hazra, A. Bhattacharjee, M. Chand, K. V. Salunkhe, S. Gopalakrishnan, M. P. Patankar, and R. Vijay, Ring-resonator-based coupling architecture for enhanced connectivity in a superconducting multiqubit network, *Phys. Rev. Appl.* **16**, 024018 (2021).
- [49] T. Ray, A. Dey, and M. Kulkarni, Localization and delocalization in networks with varied connectivity, *Phys. Rev. A* **106**, 042610 (2022).
- [50] V. Eisler and Z. Rácz, Full counting statistics in a propagating quantum front and random matrix spectra, *Phys. Rev. Lett.* **110**, 060602 (2013).
- [51] M. Inguscio, W. Ketterle, and C. Salomon, *Ultra-cold Fermi Gases* (IOS Press, Amsterdam, 2008), Vol. 164.
- [52] F. Dalfovo, S. Giorgini, L. P. Pitaevskii, and S. Stringari, Theory of Bose-Einstein condensation in trapped gases, *Rev. Mod. Phys.* **71**, 463 (1999).
- [53] J. A. Joseph, J. E. Thomas, M. Kulkarni, and A. G. Abanov, Observation of shock waves in a strongly interacting Fermi gas, *Phys. Rev. Lett.* **106**, 150401 (2011).
- [54] L. W. Cheuk, M. A. Nichols, M. Okan, T. Gersdorf, V. V. Ramasesh, W. S. Bakr, T. Lompe, and M. W. Zwierlein, Quantum-gas microscope for fermionic atoms, *Phys. Rev. Lett.* **114**, 193001 (2015).
- [55] E. Haller, J. Hudson, A. Kelly, D. A. Cotta, B. Peaudecerf, G. D. Bruce, and S. Kuhr, Single-atom imaging of fermions in a quantum-gas microscope, *Nat. Phys.* **11**, 738 (2015).
- [56] M. F. Parsons, F. Huber, A. Mazurenko, C. S. Chiu, W. Setiawan, K. Wooley-Brown, S. Blatt, and M. Greiner, Site-resolved imaging of fermionic Li 6 in an optical lattice, *Phys. Rev. Lett.* **114**, 213002 (2015).
- [57] M. Abramowitz and I. A. Stegun, *Handbook of Mathematical Functions* 10 (Dover, New York, 1972).
- [58] DLMF, *NIST Digital Library of Mathematical Functions*, companion to *NIST Handbook of Mathematical Functions*, edited by F. W. J. Olver, A. B. Olde Daalhuis, D. W. Lozier, B. I. Schneider, R. F. Boisvert, C. W. Clark, B. R. Miller, B. V. Saunders, H. S. Cohl, and M. A. McClain (Cambridge University Press, New York, 2010).